UNITED NATIONS UNIVERSITY
GEOTHERMAL TRAINING PROGRAMME
Orkustofnun, Grensasvegur 9,
IS-108 Reykjavik, Iceland

Reports 2012
Number 26

PRELIMINARY DESIGN OF THE MENENGAI PHASE I STEAM GATHERING SYSTEM

Stephen Odhiambo Onyango
Geothermal Development Company, Ltd. – GDC
P.O. Box 17700 – 20100
Nakuru
KENYA
sodhiambo@gdc.co.ke

ABSTRACT

The best piping configuration is the least expensive which offers the highest efficiency on a long term basis. This requires the consideration of installation cost, pressure loss effects on production, stress level concerns, fatigue failures, support and anchor effects, stability, expansion capacity, and easy maintenance, among others. The objective of this study is to design a steam gathering system which will provide an efficient arrangement to supply steam to four 100 MWe geothermal power plants while re-injecting all the excessive brine. In this study, three different scenarios based on different power plant locations are presented and analysed and the optimum pipeline configuration is selected considering minimal cost and pressure drop. In sizing two-phase flow pipelines, the superficial steam velocity has been restricted to a maximum of 40 m/s while the pipeline layout is carefully selected such that the flow is downwards. A minimum upward flow of 1% is allowed in two-phase pipelines in cases where the two-phase flow has to go uphill; this reduces the possibility of slug flow regimes in the pipelines.

The results show that building power plants in the same location offers the most efficient gathering system in terms of cost comparison, followed by the next best scenario of having power plants in two locations. The study has shown that it may be difficult to have centralized separator stations for all the wells due to high costs as a result of longer pipelines from some of the locations.

1. INTRODUCTION

Kenya is endowed with a large high-temperature geothermal potential, estimated at between 7,000 and 10,000 MWe, which is largely unused. In tandem with this and to capture the spirit of Kenya's vision for 2030, the country has developed an expansion plan for low-cost geothermal projects that will provide an additional 5,000 MWe by 2030 (Ngugi, 2012).

The Geothermal Development Company (GDC) was formed in 2009 with a mandate of accelerating geothermal energy production in Kenya. Currently, GDC is carrying out drilling activities within the Menengai caldera. Menengai is located within a region of the intra-continental crustal triple rift junction. This is where the Nyanzian rift joins the main Kenya rift (Simiyu, 2009). The Menengai complex is dominated by a central volcano, approximately 12 km in diameter. The caldera has steep

sides, up to 300 m high, where older shield lavas are exposed (Muchemi 1998). The field is estimated to have a potential of over 700 MWe (Ofwona, 2004). GDC started drilling in the Menengai field in 2011 with the first well (MW-01) discharging on April 2011. Several wells have been drilled and various tests and measurements conducted to evaluate the production potential of the field.

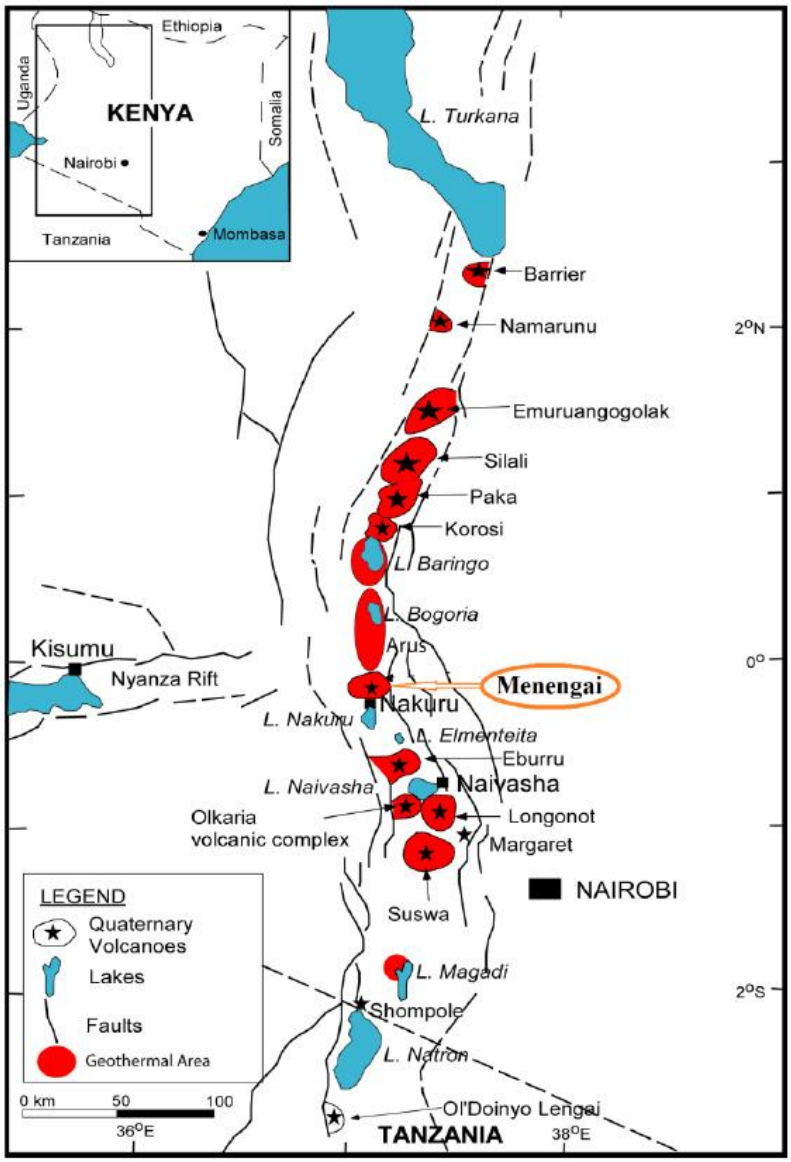

FIGURE 1: A map showing location of Menengai geothermal field and other high-temperature geothermal fields in Kenya

GDC plans to develop 400 MWe by 2016 for the first phase of development of the field. This development involves drilling and testing 102 production, injection and monitoring wells that will provide steam for the four 100 MWe power plants. Discharge well test data for three wells are available. Wellhead pressures for the wells vary and the pressure will be chosen for each well to maximize the steam flow rate. Other assumptions will be made since necessary discharge data is not available and future wells will be assumed to have the same characteristics and output as the existing wells. Figure 1 shows the location of Menengai geothermal field.

The aim of this project is to propose the best steam handling system that can be designed to supply the required amount of steam to the power plants as well as to transport separated water (brine) to the re-injection wells. The basic concept of geothermal piping design is to safely and economically transport steam, brine, or two-phase fluid to its destination with acceptable pressure loss. The best pipe configuration is the least expensive over a long term basis. Consequently, the main goal is to keep the pipeline route as short as possible, to minimize costs and lower pressure drop. All possible locations for the power plants and possible separator layouts will be considered in this design and different options compared based on cost. The goal is also to maximize the use of centralized separator stations, to be sited at locations that are carefully selected based on consideration of existing, planned and future wells locations as well as brine re-injection requirements. Several assumptions are made in this report since well drilling and testing are still on-going and some well parameters may change in the future. A rational design of any kind of construction involves knowledge of:

- The external forces to be resisted, transformed or transmitted;
- The resulting internal stresses; and
- The mechanical properties of the materials to be employed to accomplish the object sought.

2. THEORY OF PIPELINE DESIGN

A standard design process for geothermal fluid pipelines involves the following steps:

- Topology and route selection;
- Demand and flow analysis;
- Pipe diameter optimization, based on minimum cost due to head loss;
- Thickness and pressure classes;
- Mechanical stress analysis; supports types and distances;
- Thermal stress analysis, anchors, expansion loops and expansion units;
- Pump size and arrangement.

2.1 Route selection

Two methods could be used for route selection*: Cost modelling comparison* and *distance transform* (Jónsson, 2012). Distance transform will be used in this design to find optimal paths across physical landscapes for pipelines carrying two-phase geothermal fluids. The objective will be to obtain a pipeline design with minimum capital and operational costs.

The shortest distance between the start and end of a pipeline will be chosen while avoiding high and low areas as much as possible. The pipeline may be buried underground or erected above ground. Buried pipelines are expensive to construct and difficult to access and thus will not be considered an option in this study. Some of the basic items to consider for surface pipeline configurations are:

- The pipeline route should be as short as possible or with the lowest cost. Avoid unnecessary crossing of roads, rivers, restricted areas and minimize inclines. Steep slopes may result in undesirable flow regimes in the pipeline (e.g. slug flow conditions for two-phase flows) and the installation of drains at low points because of an upward incline may result in a pressure loss or pressure lower than the saturation pressure.
- All portions of the pipeline should be accessible; this reduces time in transportation and installation of pipeline components.
- Routing the pipeline over moderately inclined terrains makes it easier to construct. High inclines may be used though, but not too much.
- Avoid crossing federal or state land as the necessary permits required can delay the project.
- Avoid landslide areas and avoid crossing water courses that are eroding in order to help maintain pipeline integrity.
- The pipeline route should be selected to minimize environmental and visual effects. Here it can be mentioned that the project is located in a national game reserve.
- The possibility of a future expansion to the pipeline system should be considered.
- The route with minimum total updated costs should be considered.

2.1.1 Distance transform

A *distance transform* is an image processing algorithm for digital images. Standard distance transform works with a binary digital image that consists of object points and non-object points. In its simplest form, a distance transform obtains the distance from a point to the closest object point for each non-object point in an image.

Variable topological distance transform can be used to calculate distances over 3-D surfaces. The handling of design and land-use constraints in variable topological distance transform, such as a maximum gradient, curvature and restricted areas is straightforward to implement. With all these constraints taken into account, the variable topological distance transform method can find the shortest

route that satisfies the design values. This is of great use since most route designs are the result of ad hoc trial and error methods. This can be a powerful and easy-to-use tool.

A *digital elevation model* (DEM) is a digital representation of a given ground topography. Each grid point in a digital elevation model matrix will have longitude, latitude and altitude values. The model can range in size from a couple of hundred to millions of grid points, depending on the size of the represented area and the resolution (distance between grid points). If the resolution and accuracy of the DEM is increased, the footprint of the area represented by each grid point gets smaller. This, in turn, allows for more detailed and accurate studies of the area while reducing altogether the need for interpolation between grid points.

The variable topological distance transform method incorporates the height difference between data points into its calculations. All the cells have heights (altitudes) assigned to them and these values are used to calculate the length between cells in a 3-D space utilizing slope distance. A variable topological distance transform algorithm offers a way to obtain the shortest path by using distance transforms on digital elevation models and introducing constraints.

2.2 Two-phase flow

In geothermal pipelines, simultaneous flow of liquid water, steam and gases exists in most cases. However, since the gases are only a small fraction of the total flow, it is a safe assumption to disregard the gases and regard it as only a single component of the two-phase flow. In geothermal pipelines, the two-phase flow is assumed to be isothermal and adiabatic since the pipes are well insulated and pressure drop is relatively small compared to the total pressure in the pipeline.

Two-phase flow is highly sensitive to small changes and many experiments have been conducted to try to determine the relationship between the flow and its different properties. It has been shown that two-phase flow is highly dependent on the pipe diameter (d), pipe inclination (Δz), absolute pressure of flow (P), density of the phase (ρ_p), dynamic viscosity (μ), surface tension of the liquid (σ) and mass flow of the phases ($\dot{m}$). These properties affect the way the two phases interact and, therefore, determine the overall outlook of the frictional surface between the pipe wall and the phases. This high dependence on many different factors makes it difficult to derive a general two-phase flow analysis model for the whole range of flow conditions.

2.2.1 Flow regimes in two-phase pipelines

The complex interaction between the phases in two-phase flow forms an overall outlook of the flow each time, and this overall outlook is categorized into different flow regimes. These flow regimes have been categorized by visual inspection of the flow. The number of flow regimes that can exist in a two-phase flow is not exactly known due to the fact that the shift between regimes can become very unclear. A flow regime is a subjective and qualitative concept; therefore, it is not possible to incorporate it into mathematical equations as a parameter. The flow regimes can be categorized into several main categories by the type of flow, but these main categories and their sub-categories are still debatable. The different subcategories of the flow can differ so significantly that they cannot be ignored in a detailed analysis of the two-phase flow. The simplest classification of flow regimes is to use three regimes: separate flow, intermittent flow and distributed flow.

Thome (2006) defined seven main flow regimes in horizontal co-current flow (flowing in same direction) in which three belong to a so called intermittent flow regime, which is complex and can be very difficult to measure and predict. The division of flow is as follows and the flow regimes can be seen in Figure 2:

Dispersed bubble flow: Gas bubbles are dispersed in the liquid with a high concentration of bubbles in the upper half of the tube due to their buoyancy. The flow usually occurs at high mass flow rates in horizontal pipelines.

Stratified flow: Complete separation of the two phases occurs. It occurs at low gas and liquid velocities.

Stratified wavy flow: When gas velocity increases in a stratified flow, waves are formed on the interface and travel in the direction of flow, however the crests of the waves do not reach the top of the pipe.

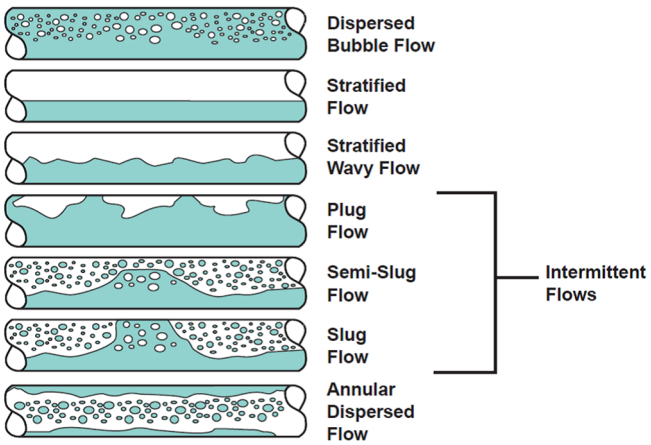

FIGURE 2: Flow regime classification (Chexal et al., 1999)

Annular flow: At even larger gas flow rates, the liquid forms a continuous annular film around the pipe perimeter. The liquid film is thicker at the bottom than the top of pipe because of gravity. The interface between the liquid annulus and gas core is disturbed by small amplitude waves and droplets may be dispersed in the gas core.

Intermittent flow: This occurs at higher velocities where the interfacial waves become large enough to reach the top of the pipe. Intermittent flow is a composite of *plug flow* and *slug flow*.

Plug flow: The liquid plugs are separated by elongated gas bubbles. The diameters of the elongated bubbles are smaller than the tube such that the liquid phase is continuous along the bottom of the tube below the elongated bubbles. It also called elongated bubble flow.

Slug flow: Is defined as frothy slug waves which reach the top of the pipe. The diameter of the elongated bubbles is similar in size to the channel height. The slug can cause a lot of difficulty because of the sudden pressure pulses and vibrations of the pipes. In reality, it is very difficult to distinguish between plug and slug flow.

Semi-slug flow: The slug waves do not reach the top of the pipe and pass through the pipe as waves. (Similar to wavy annular flow.)

The most common way to determine the flow regime of a two-phase flow is by using the so called empirical flow regime maps. Empirical flow regime maps are plots of the transition lines between each flow regime with regard to some flow parameters. These plots are correlated from measurements of the two-phase flow, coupled with some flow regime identifying techniques (Thome, 2006). Some of the flow regime maps are discussed below and will be used in this study (for original references see *Engineering data, book III* (Thome, 2006)).

Baker map: The Baker map for horizontal two-phase flow was first published in 1954 and was based on measurements from other researchers on horizontal two-phase flow of both air and water and air and oil in 1, 2 and 4 inch pipes. The Baker map is plotted with G/λ against L/ψ where G and L are mass fluxes of the gas and liquid phases, respectively, and λ and ψ are found from the following equations (Thome, 2006):

$$\Psi = \left(\frac{0.0724}{\sigma_L}\right).\left(\frac{\mu_L}{0.0009}\left(\frac{1000}{\rho_L}\right)^2\right)^{1/3} \quad (1)$$

$$\lambda = \left(\frac{\rho_G}{1.2} . \frac{\rho_L}{1000}\right)^{1/2} \quad (2)$$

The *Hoogendorn map* is one of the most used maps in praxis along with the Baker map. It was first published in 1959 and was based on measurements of two-phase air and water flow in 24-140 mm pipes. The map is plotted with respect to the entrance volume ratio as a function of the mean velocity of the total flow.

The *Breber et al. (1989) map* is the simplest map to use. It is divided into square regions, making it very easy to use. The Breber et al. map makes use of the *Martinelli* number and the *Wallis* factor as the axes; the *Wallis* factor is defined as (Thome, 2006):

$$j^* = \frac{G_L . x}{\sqrt{d . g . \rho_g (\rho_L - \rho_g)}} \quad (3)$$

And the *Martinelli* number as:

$$X = \left(\frac{1-x}{x}\right)^{0.9} \left(\frac{\rho_g}{\rho_L}\right)^{0.5} \left(\frac{\mu_L}{\mu_g}\right)^{0.1} \quad (4)$$

Plots of the Menengai pipeline results, in the Baker map, predict wavy flow; the Weisman flow regime map predicts an annular flow regime while the Mandhane et al. map predicts annular / slug flow regimes. The results are shown in Figure 3.

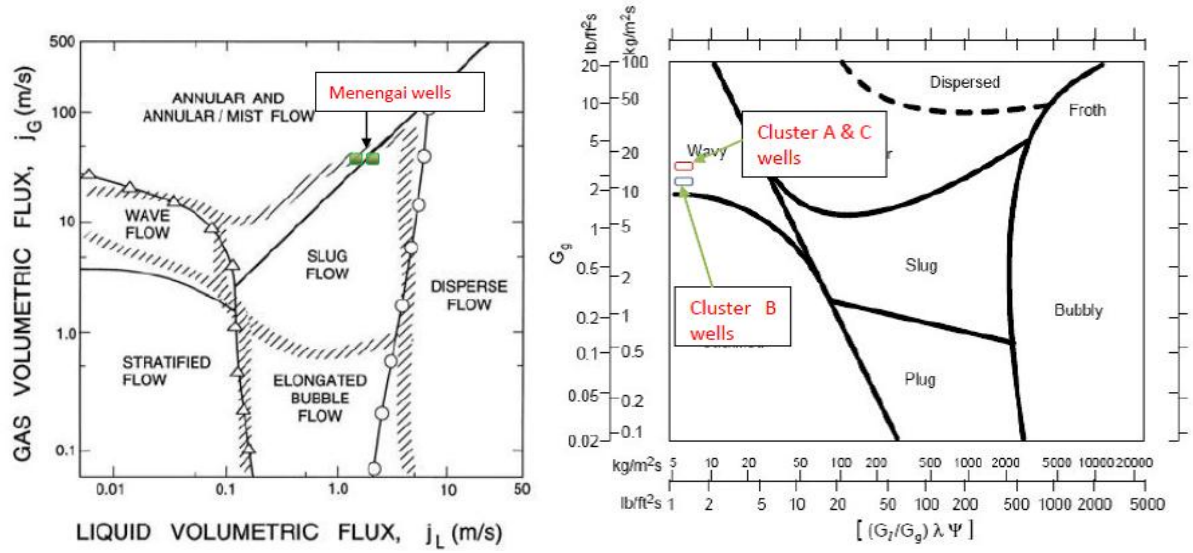

FIGURE 3: Mandhane et al. flow regime map on the left; Baker flow regime map plot on the right (Thome, 2006)

2.3 Two-phase pressure drop

2.3.1 Pressure drop due to pipeline length

Pressure drop in two-phase geothermal pipelines consists mainly of static pressure drop, momentum pressure drop and frictional pressure drop. Several different methods for calculating the pressure drop in two-phase flow in pipelines have been proposed. Separated flow models are a class of commonly utilized models (Thome, 2006) for calculating the two-phase pressure drop; they employ two artificial pipes, one carrying the gaseous phase and the other the liquid phase. The resulting two-phase pressure drop is then calculated from the single-phase pressure drops. Varying in many of the models is the

correlation used for calculating the void fraction, which is essential in estimating the two-phase pressure drop from the single-phase calculations.

Two parameters that will be used extensively in two-phase pressure drop calculations are void fraction and mass velocity. Void fraction is the ratio of the gas flow cross-section to the total cross-section.

$$\alpha = A_g/A \tag{5}$$

where A_g = Area of steam or gas;
A = Total area.

The Zhao et al. (2000) correlation will be used in estimating the void fraction. It uses the seventh power law:

$$\frac{1-\alpha}{\alpha^{7/8}} = \left[\left(\frac{1}{x}-1\right)\left(\frac{\rho_g}{\rho_f}\right)\left(\frac{\mu_l}{\mu_g}\right)\right]^{7/8} \tag{6}$$

The average liquid-phase velocity and the wall friction factor were first introduced to predict two-phase pressure drop using the techniques developed for single-phase flows. But Zhao et al. (2000) extended the idea to the pseudo flow since that flow has the same boundary layer velocity distribution as the two-phase liquid layer. A correction factor was introduced in determining the liquid-phase velocity ($\overline{V}_l$).

$$\overline{V}_l = 1.1\,(1-x)\frac{W(1-x)}{\rho_l(1-\alpha)A} \tag{7}$$

where $1.1\,(1-x)$ = A correction factor mainly for entrainment;
W = Total mass flow rate;
x = Steam quality;
ρ_l = Density of water (kg/m^3).

The average velocity of the equivalent single-phase flow can be calculated using the equation:

$$\frac{\overline{V}_l}{\overline{V}} = \frac{(1-\sqrt{\alpha})^{8/7})(1+\frac{8}{7}\sqrt{\alpha})}{(1-\alpha)} \tag{8}$$

The mixture density (ρ_{tp}) is calculated by the equation:

$$\rho_{tp} = \rho_g\alpha + \rho_l(1-\alpha) \tag{9}$$

where ρ_g and ρ_l represent the densities of the gas and liquid phases.

Two-phase dynamic viscosity (μ_{tp}) is defined as:

$$\mu_{tp} = \mu_g x + \mu_l(1-x) \tag{10}$$

where μ_g and μ_l are the viscosities of the gas and liquid phases.

Based on the average velocity of the equivalent single phase, the Reynolds number and two-phase friction factor can be calculated using the equation:

$$Re = \dot{m}_v D_{in}/\mu_{tp} \tag{11}$$

where $\dot{m}_v$ = W/A.

The friction factor is then given by:

$$f_{tp} = \frac{0.316}{Re^{0.25}} \tag{12}$$

The combined momentum and frictional pressure drop due to pipe length (ΔP_L) can be calculated by (Zhao et al., 2000):

$$\Delta P_L = \frac{f\,\rho_l \overline{V^2}}{2\,D_{in}(1-AC)}.L \tag{13}$$

where ΔP_L = Pressure drop due to length (Pa);
AC = Acceleration correction, $AC = \dot{m}_g/\rho_g p A^2 \alpha$;
$\dot{m}_g$ = Mass flow rate of steam or gas (kg/s);
p = Pressure in the pipeline (Pa);
A = Inner area of pipe (m^2).

Pressure drop due to elevation difference (static head) is calculated by:

$$\Delta P_s = \rho_{tp}\, g\, \Delta_Z \tag{14}$$

where ΔZ = The elevation difference between end and start points, $\Delta Z = H_e - H_s$.

2.3.2 Pressure drop in different installations

Because of the flow complexity, it is difficult to model the two-phase flow through a bend to derive correlations analytically, and to provide a systematic calculation method for pressure drop across a bend. As a result, many proposed correlations for predicting pressure drops in bends are empirical.

Pressure drop in bends and other installations for two-phase flow is calculated using the classic B-type two-phase multiplier method (Chisholm, 1983). The first two-phase multipliers (φ^2_{BLO}) are:

$$\varphi^2_{BLO} = 1 + \left(\frac{\rho_l}{\rho_g} - 1\right)(B\,x\,(1-x) + x^2) \tag{15}$$

where x = The steam quality;
B = $1 + 2.2/(K_{BLO}\,(2 + \frac{r}{D_{in}}))$;
K_{BLO} = Equivalent to 1.6 f h;
h = The equivalent length (m);
r = The bend radius (m).

The general pressure drop for bends, expansion units, valves and connections is:

$$\Delta P_I = \frac{f\rho_{tp}\overline{V^2}}{2}\,(\varphi^2_B n_b h_b + \varphi^2_C n_c h_c + \varphi^2_E n_u h_u + \varphi^2_V n_v h_v) \tag{16}$$

where ΔP_I = Pressure drop for the installation (Pa);
ρ_{tp} = Density;
$\varphi^2_B n_b h_b$ = Two-phase multiplier for bends;
$\varphi^2_C n_c h_c$ = Two-phase multiplier for connections;
$\varphi^2_E n_u h_u$ = Two-phase multiplier for expansion units;
$\varphi^2_V n_v h_v$ = Two-phase multiplier for valves.

Finally, the total pressure drop (Δp_T) can be calculated from the following equation:

$$\Delta p_T = \Delta P_s + \Delta P_L + \Delta P_I \tag{17}$$

2.4 Pipe diameter optimization for single-phase flow

Optimizing pipe diameter for single-phase flow (water or steam) requires considering the maximum allowable velocity in the pipe, and minimizing the total updated cost.

The total updated cost (C_t) is:

$$C_t = C_c + C_e\,(1- 1/\,(1+i)^{\,T}\,)\,/i \tag{18}$$

where C_c = Capital cost;
C_e = Annual cost;
T = Life time;
i = Interest rate.

The capital cost is equal to:

$$C_c = L_p k_p + n_b k_b + n_c k_c + n_u k_u + n_v k_v + n_d k_d + L_p k_i \tag{19}$$

where L_p = Pipe length (m);
k_p = Cost of pipe (USD/m);
n_b = Number of bends;
k_b = Cost of a bend (USD/m);
n_c = Number of connections;
k_c = Cost of a connection (USD/m);
n_u = Number of expansion units;
k_u = Cost of an expansion unit (USD/m);
n_v = Number of valves;
k_v = Cost of a valve (USD/m);
n_d = Number of pumps;
k_d = Cost of a pump (USD/m);
k_i = Cost of insulation material (USD/m)

The annual cost is calculated as:

$$C_e = k_e\, O_h\, P \tag{20}$$

where k_e =Cost of electrical energy (USD/hour);
O_h = Operating hours in one year = 8760 hours;
P = Power of the pump (W).

The pump power is calculated using the equation:

$$P = g\,\rho\,H_f\,Q/\eta \tag{21}$$

where g = Gravitational constant (m^2/s);
ρ = Density of fluid (kg/m^3);
Q = Volumetric flow rate (m^3/s);
H_f = Frictional head (m);
η = Pump efficiency.

In order to calculate the frictional head (H_f), the velocity of the fluid (V) must be calculated using equation:

$$V = Q/\left(\frac{\pi\, D_{in}^2}{4}\right) \tag{22}$$

where V = Fluid velocity (m/s);
D_{in} = Pipe inner diameter (m).

The second equivalent length (Le) can be calculated using equation:

$$L_e = L_p + n_b h_b D_{in} + n_c h_c D_{in} + n_u h_u D_{in} + n_v h_v D_{in} \quad (23)$$

where L_p = Pipe length (m);
D_{in} = Pipe inner diameter (m);
h_b = Equivalent length of bends;
h_c = Equivalent length of connections;
h_u = Equivalent length of expansion units;
h_v = Equivalent length of valves.

The Reynolds number, R_e is calculated by the equation:

$$R_e = V D_{in} / v \quad (24)$$

where v = Kinematic viscosity of fluid.

Based on the amount of the Reynolds number, the friction factor (f) should be calculated from one of the following equations (DiPippo, 2007):

$$R_e \leq 2100, \qquad f = 64/R_e \quad (25)$$

$$R_e > 5000, \quad f = 0.25/\left(\mathrm{Log}_{10}\left[\frac{\epsilon}{3.7 D_{in}} + \frac{5.74}{R_e^{0.9}}\right]\right)^2 \quad (26)$$

where ϵ = Absolute roughness.

Friction head is then calculated using the equation:

$$H_f = f V^2 \frac{L_e}{2 g D_{in}} \quad (27)$$

where H_f = Friction head (m of fluid);
f = Friction factor;
L_e = Equivalent length (m).

Pump pressure (P_p)can be calculated according to equation:

$$P_p = (\Delta Z + H_f)\, \rho\, g \quad (28)$$

where P_p = Pump pressure (Pa);
ΔZ = Elevation difference between end and start points ($\Delta Z = H_e - H_s$).

For each diameter, the total updated cost will be calculated based on the above equations. Total updated cost is the main parameter for selecting the optimum diameter as shown in Figure 4. When the diameter increases, the total capital cost increases but the updated annual cost decreases. There is an optimum diameter with minimum total updated cost. For steam lines and brine lines where brine flows by gravity (i.e. no pumping required), the diameter will be selected based

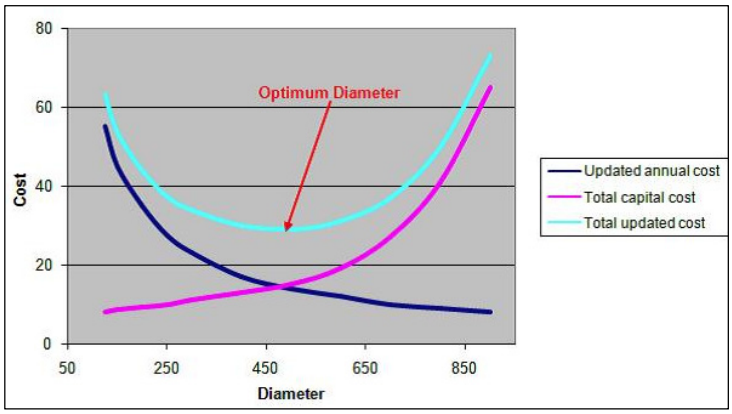

FIGURE 4: Optimum diameter selection based on minimum total updated cost

on the allowable velocity to avoid erosion of the pipeline. The velocity should be less than 3 m/s for water lines and less than 40 m/s for steam lines.

2.5 Design of separators

The optimal separator design is the one where the separation process leads to a condition where all water containing dissolved solids is removed from the steam phase. The outlet steam quality and the pressure drop are the main criteria for designing separators. The separators can be located at the wellhead, at the satellite stations in the field or at the power station. Separators are usually characterized by orientation as either vertical or horizontal (DiPippo, 2007). Regardless of shape, separation vessels usually contain four major sections plus the necessary controls:

a. *Inlet device* - It reduces the momentum of the inlet flow stream, performs an initial bulk separation of gas and liquid phases and enhances gas flow distribution.
b. *Gas gravity separation* - It is designed to utilize the force of gravity to separate entrained liquid droplets from gas phases, and precondition the gas for final polishing by the mist extractor. At this portion, the gas moves at relatively low velocity with little disturbance.
c. *Liquid gravity separation* - Acts as a receiver for all liquid removed from the gas inlet, gas gravity and mist extraction sections. This section provides residence time for degassing the liquid. Depending on the inlet flow characteristics, the liquid section should have a certain amount of surge volume or slug catching capacity to smooth out the flow passes on the downstream equipment processes.
d. *Mist extraction* - It utilizes a mist extractor that consists of a knitted wire mesh pad, and a series of vanes or cyclone tubes. This section removes the very small droplets of the liquid from gas by impingement on a surface where they coalesce into larger droplets or liquid films.

When selecting a separator, there are several design parameters that should be taken into account. These are some of the parameters:

- Steam quality of the separated steam;
- Steam pressure drop;
- Facility of operation and cleaning;
- Cost.

A Webre type separator will be used in this study since it is simple with no moving parts that can be corroded or eroded. A separator with a spiral inlet is more efficient than a tangential inlet. By progressively increasing the inlet velocity, the separation efficiency increases until a breakdown velocity is reached. Above this velocity, the efficiency deteriorates rapidly. The spiral inlet separator has a higher inlet breakdown velocity than a tangential one (about 60% higher). The spiral inlet separator achieves the highest efficiency when the steam inlet velocity is between 30 and 40 m/s. The breakdown velocity is approximately 45 m/s (Lazalde-Crabtree, 1984).

In the Webre cyclone, the steam first moves in a spiral pattern to the top and then changes direction by 180° to go down and out the bottom outlet. Since both steam and water outlets are at the bottom of the cyclone, piping layouts are simple as they are conveniently located relatively near ground level, as opposed to the top of a separator that may be up to 20 m high. They are also easy to clean; it is recommended to schedule at least a general maintenance per year for wellhead separators. The outlet steam quality and efficiency are very high. The reported steam quality (dryness) has an average which is higher than 99.99% at Cerro Prieto, Mexico.

2.5.1 Design parameters

The inlet should be a spiral with constant curvature and a small downward angle on the inlet to encourage brine to spiral downwards. The outlet liquid pipe (D_b) should be equal to the inlet mixture pipe

diameter (D_t). The steam outlet pipe (D_e) should be equal to the inlet pipe diameter. The separator should include a water drum which can be either integrated or not. This drum acts as a capacitor to give smooth operation and as a water-seal to avoid steam losses. A drawing of a typical vertical geothermal separator is shown in Figure 5 and recommended design parameters in Table 1.

TABLE 1: Recommended design parameters for geothermal separators (Lazalde-Crabtree, 1984)

Parameter	Recommended value for separator design
Maximum steam velocity at inlet mixture pipe	45 m/s
Steam velocity range at inlet mixture pipe	25-40 m/s
Maximum annular upward steam velocity inside cyclone	4.5 m/s
Upward steam velocity inside cyclone	2.5-4.0 m/s
α	$0.15\times D_t$
β	$3.5\times D_t$
z	$5.5\times D_t$

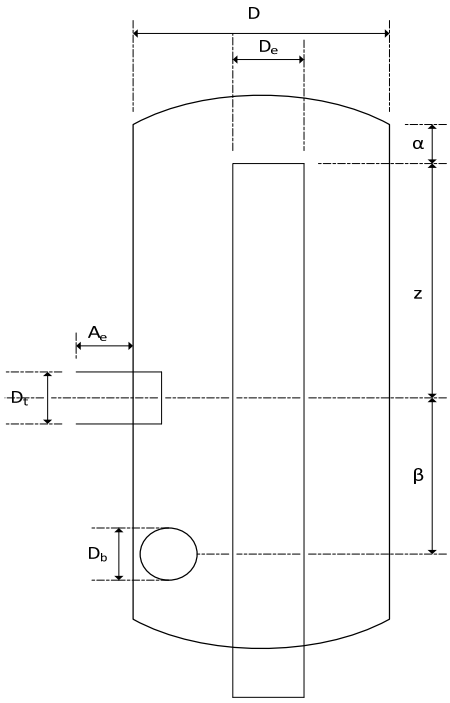

FIGURE 5: Sketch of a vertical geothermal separator

2.5.2 Separation efficiency

The separator efficiency is measured by the amount of brine carried over into steam. The efficiency is the product of mechanical (centrifugal) and annular efficiency. It is well known that the efficiency of a cyclone is reduced when the drop diameter decreases; therefore, one should understand the causes and reasons for an increase or a reduction in droplet diameter.

$$\eta_{ef} = \eta_m * \eta_A \tag{29}$$

where η_{ef} = Efficiency of separation;
η_m = Centrifugal efficiency;
η_A = Annular (entrainment) efficiency.

$$\eta_{ef} = \frac{M_L - M_A}{M_L} \tag{30}$$

where M_L = Mass of inlet liquid;
M_A = Mass of outlet liquid.

The outlet steam quality is defined as:

$$x_o = \frac{M_G}{M_G + M_A} \tag{31}$$

Substituting M_A in the efficiency equation,

$$x_o = \frac{M_G/M_L}{1 - \eta_{ef} + M_G / M_L} \tag{32}$$

If $\eta_{ef} = 0$ then x_o is the inlet steam quality. If, on the other hand, $\eta_{ef} = 1$, then $x_o = \eta_{ef} = 1$, which is the only case where $x_o = \eta_{ef}$.

With the separation pressure, all thermodynamic properties of the liquid and steam can be calculated.

2.5.3 Pressure drop in separators

A separator is a vessel used to separate a mixed-phase stream into gas and liquid phases that are relatively free of each other. They are characterized as either vertical (cyclone) or horizontal (gravity), based on orientation. Recommended inlet velocities should be in the range of 25-40 m/s, the higher the better, but may be limited by the occurrence of unacceptable pressure drop. The pressure head is estimated in terms of velocity head as follows (Walas, 1990):

$$\Delta P_{sep} = 4\ P\ \frac{V^2}{2\ g} \tag{33}$$

where V = Inlet velocity;
P = Pressure.

2.6 Pipe thickness and pressure class

The thickness of a pipe should be determined based on the pressure inside the pipe called the design pressure. This should be the pressure in the pipe under the most severe conditions in the lifetime of the pipeline. According to ASME B31.1 (1974), the nominal pipe thickness t_n is larger or equal to the required pipe thickness, t_m, according to the equation:

$$t_n \geq\ t_m = \frac{P\ D_o}{2\ (S\ E + P\ y)} + A \tag{34}$$

where P = Design pressure (Pa);
D_o = Outside diameter of pipe (m);
S = Allowable stresses (Pa);
E = Welding factor;
y = Temperature dependent co-efficient (y = 0.4 for temperature < 480°C);
A = Additional thickness due to milling and corrosion (m).

2.7 Mechanical stress analysis

2.7.1 Loads acting on the pipeline

Loads acting on a pipeline system consist of mechanical loads, thermal loads due to restraint and temperature gradients, and load effects due to supports, anchors, and terminal movement.

Mechanical loads consist of sustained loads that will weigh on the system continuously during the operating life of the pipeline system such as the weight of the pipe, insulation, pipe medium and occasional loads such as dynamic effects (impact forces due to external or internal conditions, wind and seismic loading, vibration) and weight effects (weight of medium transported and ice or snow loads, if any). Other dynamic loads that can be considered are fluid hammer effects, thrust from safety valves, and slug flow.

a. Allowable stresses

In order to calculate the distance between supports, we should know the basic allowable stresses of a pipe (S). Based on the yield limit ($R_{p/t}$) and the ultimate strength at the calculated temperature ($R_{m/T}$), allowable stresses can be calculated from the equations:

$$S = \min(R_{m/T}/3, R_{m/h}/3, 2\ R_{p/c}/3, 2\ R_{p/h}/3 \tag{35}$$

$$S_h = \min(\ R_{m/h}/3, 2R_{p/h}/3) \tag{36}$$

$$S_c = \min(R_{m/c}/3, 2R_{p/c}/3) \quad (37)$$

where S_h and S_c are basic allowable stresses during operation under hot and cold conditions, respectively.

b. Sustained loads

The following condition must be satisfied for distance between supports based on sustained loads:

$$\frac{P\,D_o}{4\,t_n} + (0.75\,i\left(\frac{M_A}{Z}\right)) \leq S_h \quad (38)$$

where I = Stress intensity factor, where $(0.75\,i) \geq 1.0$;
M_A = Sustained bending moment (Nm);
Z = Section modulus (m^3), and
Z = $\frac{\pi}{32}\left(\frac{D_o^4 - D_{in}^4}{D_o}\right)$

Vertical sustained loads

Vertical sustained loads act upon the pipeline over the entire lifetime. Vertical sustained loads (q_{sv}) include pipe weight, insulation weight and piping component weight that can be calculated. The loads can be calculated from the equations:

$$q_{sv} = q_p + q_e \quad (39)$$

$$q_p = \pi\,g\,\rho_s\left(\frac{D_o^2 - D_{in}^2}{4}\right) \quad (40)$$

$$q_e = \pi\,g\,\rho_e\left(\frac{D_e^2 - D_o^2}{4}\right) \quad (41)$$

where q_p = Pipe weight (N/m);
q_e = Insulation weight (N/m);
ρ_s = Density of steel (kg/m^3) = 7850 kg/m^3 for carbon steel pipes;
ρ_e = Density of insulation (kg/m^3) = 220 kg/m^3 for calcium silicate; and
D_e = Diameter of insulation (m).

c. Occasional loads

The following conditions must be fulfilled when occasional loads act upon a pipeline:

$$\frac{P\,D_o}{4\,t_n} + 0.75\,i\left(\frac{M_A}{Z}\right) + 0.75\,i\left(\frac{M_B}{Z}\right) \leq kS_h \quad (42)$$

where M_B = Dynamic bending moment (N/m);
k = 1.20 if load is less than 1% of operational time;
= 1.15 if load is less than 10% of operational time; and
= 1.00 else.

Vertical occasional loads:

Vertical occasional loads (q_{dv}) consist of transported medium weight, snow weight (if applicable) and seismic vertical loads that can be calculated by:

$$q_{dv} = q_v + q_s + q_{jv} \quad (43)$$

$$q_v = \pi\,g\,\rho_v\left(\frac{D_{in}^2}{4}\right) \quad (44)$$

$$q_s = 0.2\,S\,D_e \quad (45)$$

$$q_{jv} = 0.5\,e\,q_o \quad (46)$$

$$q_o = q_v + q_p + q_e \quad (47)$$

where q_v = Medium weight (N/m);
q_s = Snow weight (N/m);
q_{jv} = Seismic vertical load (N/m);
ρ_v = Density of medium (kg/m^3);
S = Snow factor (N/m^2);
e = Seismic factor.

Horizontal occasional loads:
Horizontal occasional load (q_{dh}) is the maximum value of wind or seismic load that can be calculated.

$$q_{dh} = \max [q_w, q_{jh}] \quad (48)$$

$$q_w = C\, p_w\, D_e \quad (49)$$

$$p_w = v^2 / 1.6 \quad (50)$$

$$q_{jh} = e\, q_o \quad (51)$$

where q_w = Wind load (N/m);
q_{jh} = Seismic horizontal load (N/m);
p_w = Wind pressure (N/m^2);
C = Form factor, C = 0.6 for pipe; and
v = Maximum wind speed (m/s).

2.7.2 Bending moment

The pipeline is assumed to be a simple beam between two supports. Thus, the bending moment at each support can be calculated by (Jónsson, 2012):

$$M_A = q_{sv} \frac{L_s^2}{8} \quad (52)$$

$$q_{jh} = e\, q_o M_B = \sqrt{(q_{dv}^2 + q_{dh}^2)} \,.\, (\tfrac{L_s^2}{8}) \quad (53)$$

where M_A and M_B= Sustained bending moment and dynamic bending moment (Nm), respectively;
L_s = Distance between two supports (m).

2.7.3 Length between supports

When the pipe is installed above the ground, it is supported as shown in Figure 6.

The pipe supports shall be located at the point where the support can sustain a portion of the weight of the piping system plus any superimposed vertical loads. The length between supports (L_s) shall fulfil the following conditions:

$$L_s^2 \leq \frac{\left[k\, S_h - \frac{P\, D_o}{4\, t_n}\right]\left[\frac{\pi}{4}\left(D_0^4 - D_{in}^4\right)\right]}{\left[D_o(0.75\, i)\left\{(q_{sv}) + \left(\sqrt{q_{dv}^2 + q_{dh}^2}\right)\right\}\right]} \quad (54)$$

FIGURE 6: Horizontal supports on the left and pipe supports on the right

2.8 Length between horizontal and vertical supports

Pipe supports on expansion loops consist of two types. Horizontal supports allow the pipe to move axially (in the direction of the pipe) while vertical supports allow the pipe to move both axially and radially (in the direction perpendicular to the pipe). Horizontal length between supports depends on the expansion arm. The vertical span equals the distance between supports (L_{sv}), while the horizontal span equals the arm of the loop along the pipeline (L_{sh}). The lengths between these two kinds of supports must be selected to meet the following conditions (Jónsson, 2012):

$$(0.75\ i)\left\{(q_{sv}L_{sv}^2) + \left(\sqrt{(q_{dv}L_{sv}^2)^2 + \left(q_{dh}L_{sh}^2\right)^2}\right)\right\} \leq \left(k\,S_h - \frac{P\,D_o}{4\,t_n}\right) 8\,Z \qquad (55)$$

where L_{sv} = Length between vertical supports (m), equal to length of arm;
L_{sh} = Length between horizontal supports (m).

2.9 Thermal expansion of pipeline

Geothermal pipelines carry hot fluids such as brine and steam, thereby operating at higher temperatures. It follows that they expand, especially in length, with an increase from ambient to working temperatures. This is because the pipes are installed at ambient temperatures. This expansion creates stresses upon certain areas within the pipeline network such as joints which, if extreme, could cause the pipeline to buckle. The pipe expansion (ΔL) in a pipe with the length (L) is calculated using the equation:

$$\Delta L = \alpha\, L\, \Delta T \qquad (56)$$

where α = Coefficient of thermal expansion (1/°C);
ΔT = Temperature difference (°C).

Then thermal strain (ε_x) is equal to:

$$\varepsilon_x = \frac{\Delta L}{L} = \alpha\, /\Delta T \qquad (57)$$

The thermal stresses (σ_x) and load on anchors (F) can be calculated by:

$$\sigma_x = \mathrm{E}\,\varepsilon_x \tag{58}$$

$$\mathrm{F} = \mathrm{A}\,\sigma_x \tag{59}$$

where E = Young's modulus of the pipe material ($\mathrm{N/m^2}$); and
A = The cross-sectional area on which the stress acts.

2.9.1 Expansion loops

Expansion loops are used to absorb the thermal expansion of the pipeline. Loops provide the necessary room for pipes in a perpendicular direction to absorb thermal expansion. Expansion loops prevent overstress or fatigue of the pipe and pipe supports. There are several common types of expansion loops that can be used, such as zigzag or change of direction and U-shape expansion loops. Configurations featuring 'change in direction' should not be restrained by putting them up against joists, studs, walls or other structures. The selection between these types depends upon the size of the expansion loop, availability of area and cost. According to ASME B31.1 (1974), given that the piping system is of uniform size and has no more than two anchors and no intermediate restraints, then the expansion loop (both u-shape expansion loops and change of direction (zigzag) expansion loops will be evaluated here) should meet the following requirements with respect to thermal expansion:

$$\frac{\mathrm{D_o\,Y}}{(\mathrm{L}-\mathrm{U})^2} \leq 208.3 \tag{60}$$

where D_o = Outside diameter of pipe (m);
Y = Resultant movement to be absorbed by the pipe loop (mm);
L = Developed length of line axis (m); and
U = Anchor distance (m).

a. Change of direction (zigzag type) expansion loop

The change in direction method exemplified in this study will only have two anchors with no intermediate restraint. This expansion loop should meet the conditions given in the following equations with respect to thermal expansion (Jónsson, 2012). Figure 7 shows a sketch of a change of direction expansion loop.

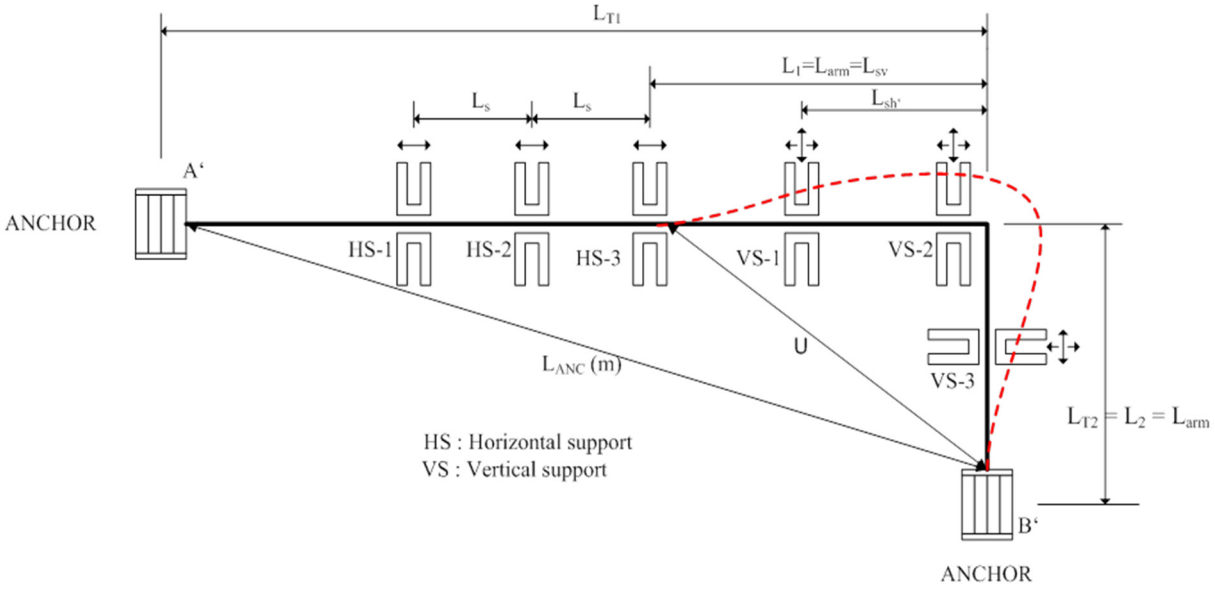

FIGURE 7: Change of direction expansion loop; the red dotted lines shows pipe deflection due to expansion

$$Y = \alpha \Delta T . \sqrt{(L_{T1}^2 + L_{T2}^2)} \quad (61)$$

$$L = L_1 + L_2 \quad (62)$$

$$U = \sqrt{L_1^2 + L_2^2} \quad (63)$$

$$L_{ANC} = \sqrt{(L_{T1}^2 + L_{T2}^2)} \quad (64)$$

Assuming $L_1 = L_2 = L_{arm}$, the above equations can be simplified to:

$$L_{arm} \geq \sqrt{\frac{D_o \alpha \Delta T L_{ANC}}{71.477}} \quad (65)$$

where L_{T1}, L_{T2} = Length between anchors on each axis (m);
L_1, L_2, L_{arm} = Length of arm (m); and
L_{ANC} = Distance between two anchors (m).

b. U-shape expansion loop

U-shape expansion loops can be vertical or horizontal. A vertical loop is used to locate the loop at a road crossing. Vertical directional supports are provided to support the weight of the calculated span. Horizontal loops (Figurer 8) need a few more supports than vertical loops in the bend length portion. There are some methods used in estimating the loop's size. The Kellogg method uses the M.W. Kellogg chart (Appendix I) to calculate the loop's size as follows (Kellogg, 1956):

The x-axis of this chart is K_2 and isolines for K_1 run across the chart. By selecting a value for either of the two parameters, K_1 or K_2, the value of the other parameter can be read from the chart; then the dimensions of the loop can be obtained by multiplying L by the parameters, as indicated in Figure 8.

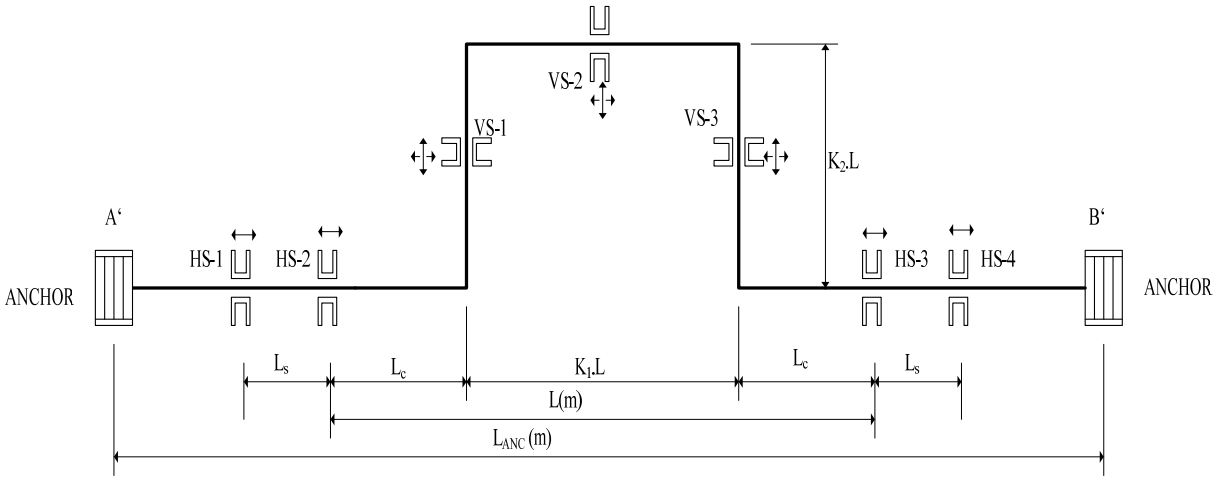

FIGURE 8: U shape expansion loop with design parameters

The distance from the guide horizontal supports to the loop (L_C) is calculated by the following formula:

$$L_C = \frac{1}{2} L (1 - K_1) \quad (66)$$

The y-axis of the chart is obtained by:

$$y_{axis} = \frac{L^2 S_A}{10^7 D_o \Delta} \quad (67)$$

where L = Length between guide horizontal supports (ft);
S_A = Allowable stress range of material (pounds/inch^2); and
Δ = Expansion from A' to B' (inch).

3. MENENGAI PIPELINE DESIGN

3.1 Design data

The field is divided into five clusters as shown in Figure 9. All production wells are in clusters A, B and C while re-injection wells are located in clusters D and E. In this design, the power plants are assumed to be located in clusters A and F.

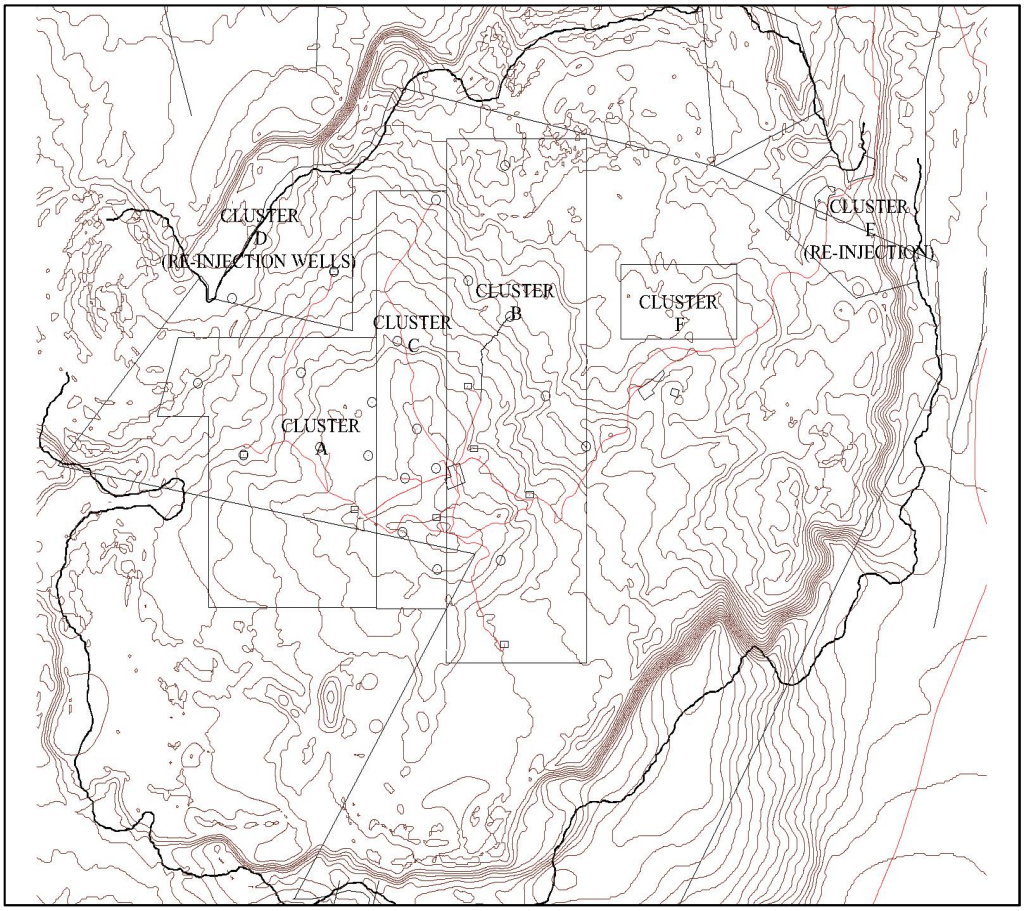

FIGURE 9: A map of the Menengai caldera showing possible well clusters

Three scenarios are evaluated in this report:

- *Scenario 1:* The power plants are located in cluster A. Two configurations for separator location are considered, i.e. central separator station in cluster A for wells in clusters A and C, and a separator station in each cluster A, B and C (hybrid and single-phase pipeline configurations).
- *Scenario 2:* The power plants are located in cluster F. Three cases are calculated depending on the locations of the separator stations, i.e. central separator stations in cluster F for all wells, central separator stations in cluster F for wells in clusters B and C, and individual separator station in each cluster A, B and C (two-phase, hybrid and single-phase pipeline configurations).
- *Scenario 3:* Two power plants, one each located in clusters A and F. The separator stations are located in each cluster and steam pipelines run to the power plants while brine pipelines go to the re-injection wells.

Tables 2 and 3 give a summary of flow discharge tests of two wells, MW-01 and MW-04, located in clusters A and B, respectively. Measured downhole temperature and pressure profiles of the wells are attached in Appendix II. Table 4 summarises the weather data.

TABLE 2: Discharge summary of well MW-01

Pipe diameter (mm)	WHP (bar-a)	Total mass flow (kg/s)	Water flow (kg/s)	Enthalpy (kJ/kg)	Steam flow at WHP (kg/s)
Set 1 (29/5/2011 – 11/7/2011)					
202	7.9	59.4	40	1155.3	14.5
155	8.3	54.6	37	1150.7	13.1
130	9.4	54.2	34.6	1234.5	15.3
104	11.9	48	31.7	1210.7	13
Set 2 (13/7/2011 – 24/8/2011)					
202	6.9	51.8	34	1195.6	13.6
155	7.4	46.7	32.5	1115.3	10.6
130	8.4	47.9	31.2	1198.8	12.6
104	10.7	44.9	29	1217.3	12.3
80	14.5	40.3	25.6	1241.6	11.5
Set 3 (25/8/2011 – 21/9/2011)					
202	6.3	45	29.1	1213.5	12.2
155	7.3	44.5	29	1208.8	12
130	8.5	45.2	29	1231.2	12.7
104	10.3	42.8	27.6	1213.9	11.6

TABLE 3: Discharge summary of well MW-04

Pipe diameter (mm)	WHP (bar-a)	Total mass flow (kg/s)	Water F low (kg/s)	Enthalpy (kJ/kg)	Steam flow at WHP (kg/s)
Set 1 (29/10/2011 – 27/12/2011)					
202	5.0	23.06	13.06	1410	8.41
155	6.5	22.22	12.78	1370	7.64
130	8.1	21.67	11.94	1428	8.05
104	11.1	20	11.11	1413	7.31
80	16.2	18.06	9.44	1501	7.39
Set 2 (29/12/2011 – 26/2/2012)					
202	4.4	21.67	13.06	1324	7.03
155	6.0	20.56	11.94	1355	6.92
130	7.4	20.56	11.67	1388	7.25
104	10.3	20	10.83	1431	7.53
80	14.9	18.33	9.72	1498	7.47

TABLE 4: Summary of weather data

Parameter	Maximum	Minimum	Average
Temperature (°C)	21.3	18	19.2
Wind speed (m/s)	5.8	3.4	4.1
Relative humidity (%)	78	44	61
Barometric pressure (bar)			0.83

Specifications of pipe material used in this study are given in Table 5.

TABLE 5: Pipe material details

Material parameter	Value
Pipe material	ASTM A53 B Seamless
Young's modulus	200×10^9 Pa
Allowable stress at operating condition	120×10^6 Pa
Corrosion allowance	3 mm
Pipe roughness	0.046 mm

3.2 General assumptions

The models generated, are based on the Engineering Equation Solver (EES) software (F-Chart Software, 2012). An example of model calculations is given in Appendix III. The following assumptions are made:

- All production wells in clusters A, B and C will have the same mass flow rates, enthalpy and wellhead pressures as wells MW-01, MW-04 and MW-06, respectively.
- Distances between wells in each cluster to the separator station in the same cluster are assumed constant for ease of calculation.
- All re-injection wells in clusters D and E will be able to accept all the brine from the separator stations.
- Cluster A provides 47% of total flow and 35% of steam flow rate at 0.25 dryness fraction.
- Cluster B provides 17% of total flow and 17% of steam flow rate at 0.36 dryness fraction.
- Cluster C provides 36% of total flow and 48% of steam flow rate at 0.47 dryness fraction.
- All power plants are located in one area for Scenarios 1 and 2.
- Costs of pipe supports and expansion loops were not considered in the economic analysis.
- The cost of the steam pipeline from separator stations to the power plants has not been calculated.
- The cost of the steel used (USD/m) is estimated from prices quoted by Kenyan steel pipes retailers.
- SI units are used in all calculations.
- The insulation thickness is 100 mm for all pipeline configurations.

3.2.1 Interface point elevations and co-ordinates

The x and y co-ordinates indicated in Table 6 are generated from an AutoCAD map used in distance transform to calculate pipeline route and length (see Appendix IV)**.**

TABLE 6: Elevations and co-ordinates of major interface points

Cluster	Elevation (m)	X coordinate	Y coordinate
Cluster A (MW-01)	2065	4850	6850
Cluster B (MW-04)	2098	6311	7515
Cluster C (MW-06)	2102	5857	6759
Cluster D	1898	4601	9478
Cluster E	1760	10431	10441
Cluster F	1860	8308	9101

3.3 Results

The results presented are based on all three possible scenarios which were calculated based on the possible locations for the power plants and separator stations.

3.3.1 Scenario 1 results – power plant in cluster A

In this scenario, only two cases were considered:

1. Central separator station for clusters A and C, and an individual separator station for cluster B – hybrid pipeline;
2. Individual separator stations at each cluster – single-phase pipeline scenario.

Table 7 shows the results of the best pipeline configuration selected for this scenario.

TABLE 7: Scenario 1, hybrid pipeline configuration scenario results

Line ID	Length (m)	Pipe diameter (mm)	Flow type	Fluid velocity (m/s)	Pressure drop (bar)	Cost (USD)	Cost (USD/kg of fluid)
A – A (Sep)	637	4×1000	Two phase	39.31	0.02	1,056,436	800
C – A (Sep)	1635	4×1000	Two phase	39.62	-0.10	2,677,268	2640
B – B (Sep)	448	2×1000	Two phase	38.14	-0.02	374,742	770
B (Sep) – A	2546	2×1000	Steam	34.51	0.64	2,078,402	11,830
A (Sep) – D	3313	2×750	Brine	1.94	-15.34	2,312,877	1403
B (Sep) – E	5045	1×500	Brine	1.63	-30.27	772,243	2472

The total cost for the selected pipeline configuration for two-phase and single-phase pipe configurations is USD **9,300,000.** When the pipe thickness for the above scenario was changed from schedule 10 to schedule 20, the total cost of the pipeline went up by USD **1,130,000** to USD **10,400,000.** Figure 10 shows two pies which give the percentage share of two-phase and single-phase pipelines as a function of the total cost, and the total cost of the pipeline in each cluster as a percentage.

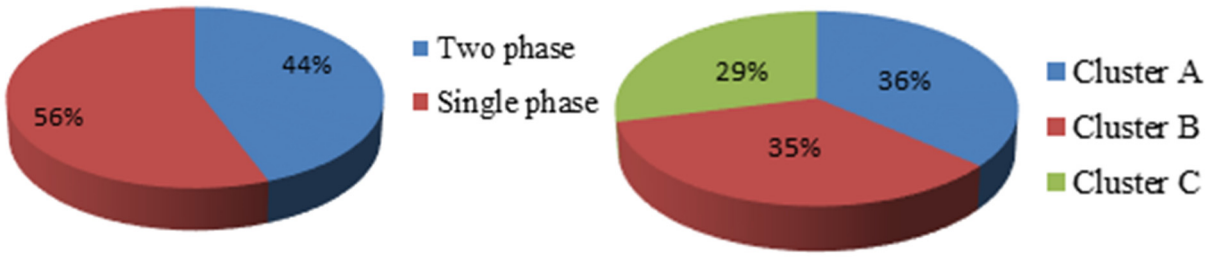

FIGURE 10: Pie charts showing percentage contribution of pipe fluid type (on the left) and of clusters (to the right)

Figure 11 shows the results in a flow chart as drawn and calculated by EES.

The results when the separator stations are located in each cluster A, B and C, are shown in Table 8.

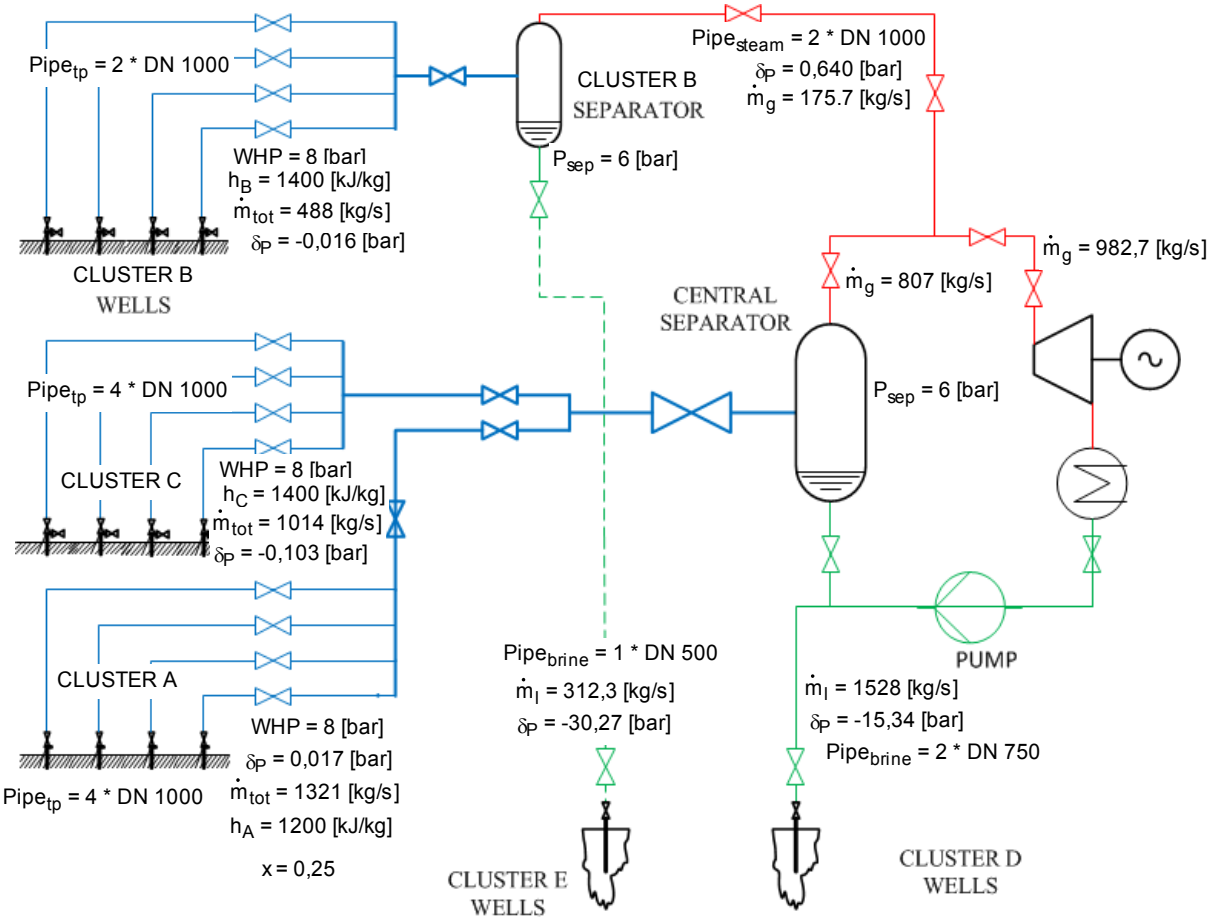

FIGURE 11: Scenario 1 results, central separator station for cluster A and C wells and an individual separator station for cluster B, drawn and calculated in EES

TABLE 8: Scenario 1, single-phase pipeline system results

Line ID	Length (m)	Pipe diameter (mm)	Flow type	Fluid velocity (m/s)	Pressure drop (bar)	Cost (USD)	Cost (USD/kg of fluid)
A – A (Sep)	637	4×1000	Two phase	39.31	0.02	1,056,436	800
B – B (Sep)	448	2×1000	Two phase	38.14	-0.02	374,742	770
C – C (Sep)	1357	4×1000	Two phase	39.62	0.10	2,225,772	2195
B (Sep) – A	2546	2×1000	Steam	34.51	0.64	2,078,402	11830
C (Sep) – A	1322	6×1000	Steam	34.25	-0.10	3,253,392	6827
A (Sep) – D	3313	1×850	Brine	1.72	-15.42	1,016,499	1337
B (Sep) – E	5045	1×500	Brine	1.63	-30.27	772,243	2472
C (Sep) – D	1805	1×700	Brine	1.91	-17.32	431,238	851

The total cost of the selected pipelines is USD **11,200,000.** The cost is higher than when a centralized separator is used for clusters A and C. Comparison of individual contributions of the clusters as a function of the pipe fluid type is presented in Figure 12.

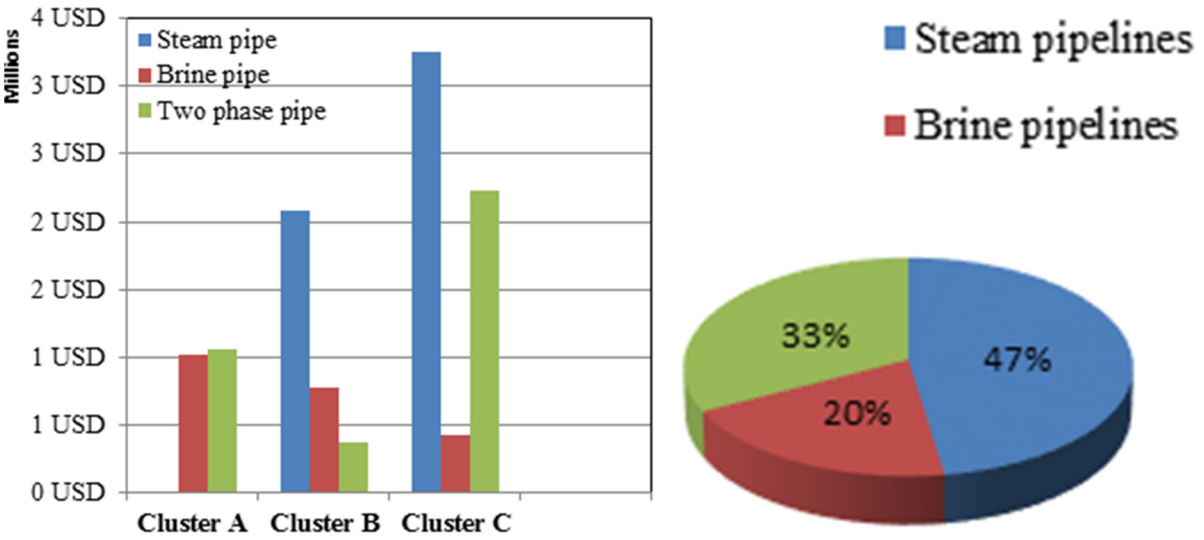

FIGURE 12: Charts showing cost for each cluster by pipe fluid type (on the left) and percentage contribution by pipe fluid type (to the right)

Figure 13 shows the results from calculations in EES.

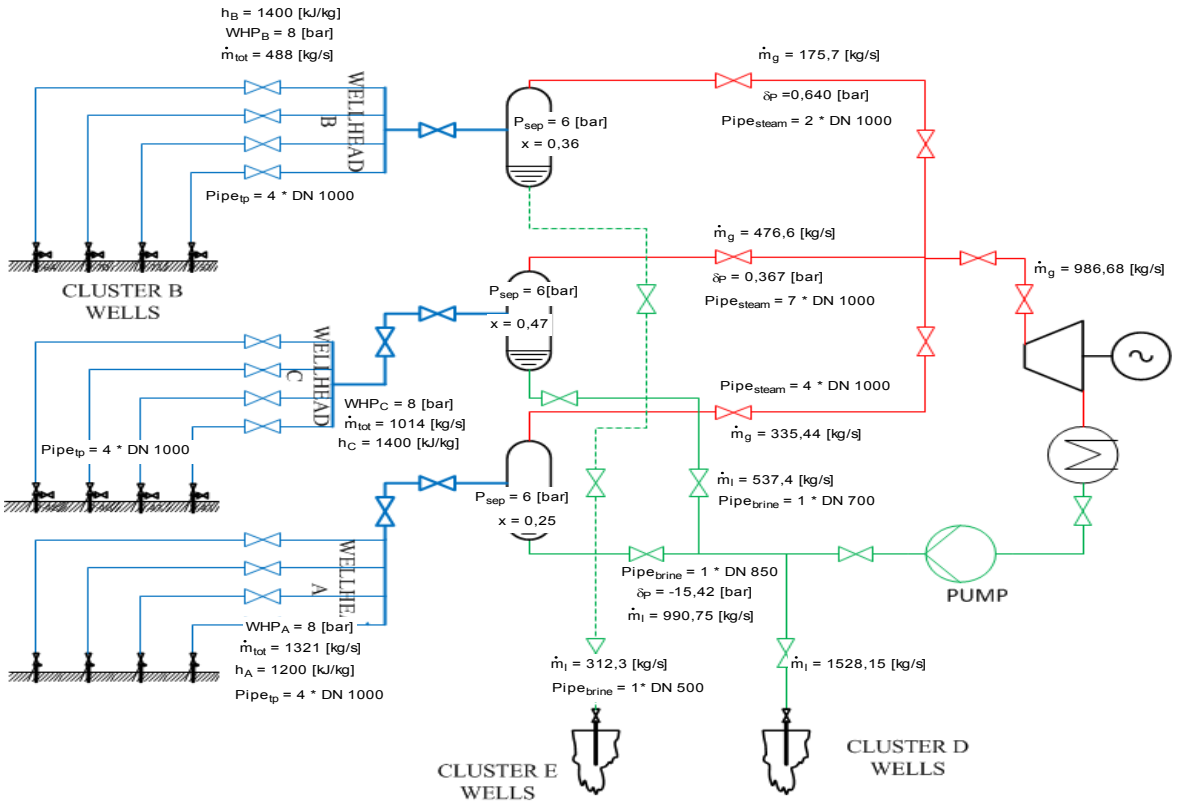

FIGURE 13: Scenario 1 results, individual separator station at each cluster A, B and C, drawn and calculated in EES

3.3.2 Scenario 2 results

In this scenario, the power plants are located in cluster F; different separator stations are considered and evaluated as shown in Tables 9, 10 and 11.

The results for a central separator station located in cluster F are shown in Table 9. It gives the most expensive pipeline construction costs due to the long pipeline routes from cluster A. The total cost for the selected pipeline configuration is USD **27,000,000.** The calculation results are also presented in Figure 14.

TABLE 9: Scenario 2, two-phase pipeline results

Line ID	Length (m)	Pipe diameter (mm)	Flow type	Fluid velocity (m/s)	Pressure drop (bar)	Cost (USD)	Cost (USD/kg of fluid)
A – F	6788	4×1000	Two phase	39.31	-1.31	11,046,152	8362
B – F	2564	2×1000	Two phase	38.14	-1.82	2,093,018	4289
C – F	7300	4×1000	Two phase	39.62	-1.21	11,877,680	11714
F – D half brine	4144	1×850	Brine	1.92	4.40	1,207,459	1367
F – E half brine	2672	1×850	Brine	1.92	-8.26	781,542	885

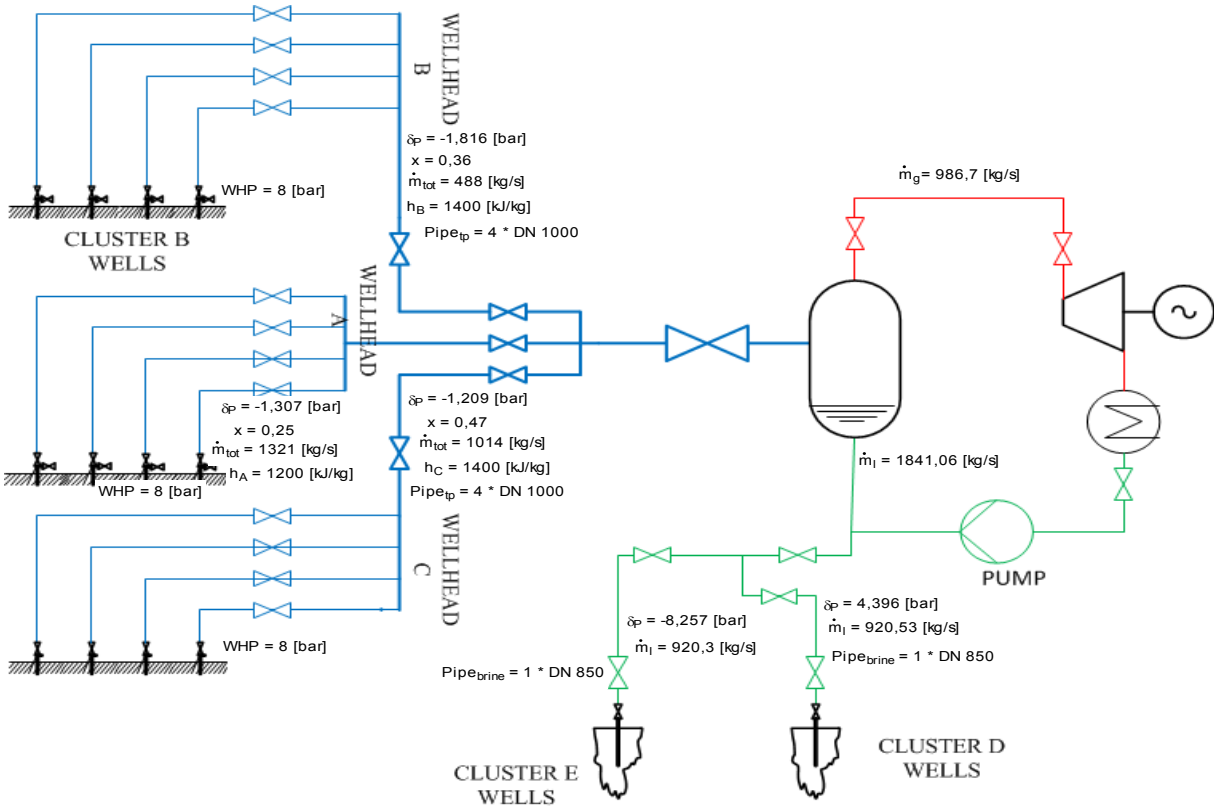

FIGURE 14: Scenario 2 results, central separator station at cluster F, drawn and calculated in EES

The results in Table 10 show when cluster A has an individual separator station, while a central separator station is located in cluster F for all wells in clusters B and C. There is a reduction in price by about 2.5 million USD compared to the case of a central separator station in cluster F for all the wells. The total cost of the entire pipeline is USD **23,500,000.** Figure 15 shows the cost contributions per cluster and contribution per type of pipe fluid type.

TABLE 10: Scenario 2, hybrid pipeline scenario – central separator station in cluster F for cluster B and C wells and individual separator station in cluster A

Line ID	Length (m)	Pipe diameter (mm)	Flow type	Fluid velocity (m/s)	Pressure drop (bar)	Cost (USD)	Cost (USD/kg of fluid)
A – A (Sep)	637	4×1000	Two phase	39.31	0.02	1,056,436	800
A – F	4789	6×900	Steam	27.82	0.78	9,418,002	28518
B – F	2564	2×1000	Two phase	38.14	-1.82	2,093,018	4289
C – F	7300	4×1000	Two phase	39.62	-1.21	8,724,080	8604
A – D	3313	1×850	Brine	1.72	-15.42	826,724	1101
F – E	2672	2×750	Brine	1.76	-8.34	1,349,880	883

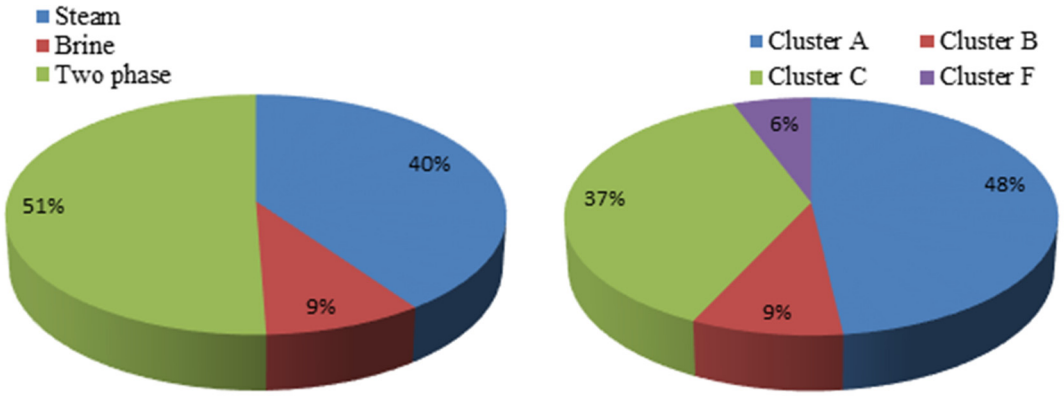

FIGURE 15: Charts showing percentage contribution per pipe fluid type (on the left) and per cluster (to the right)

The calculation results based on EES are presented in Figure 16.

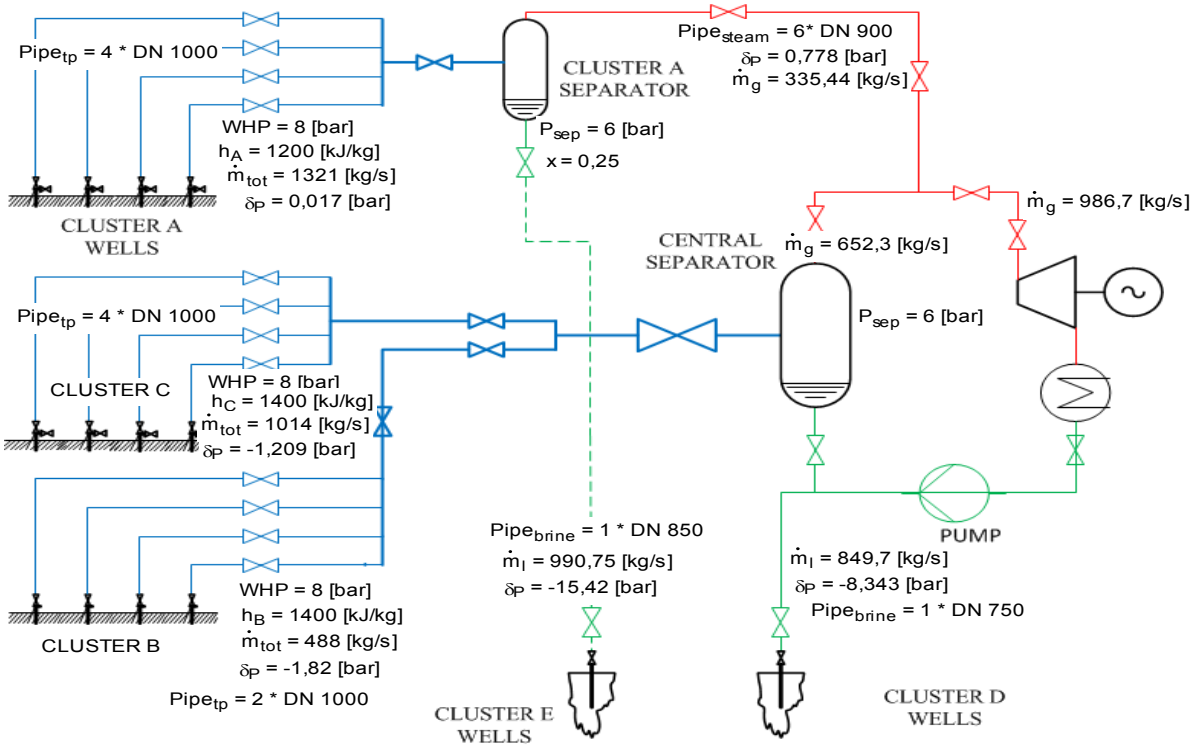

FIGURE 16: Scenario 2 results, central separator station at cluster F for cluster B and C wells, and individual separator station in cluster A, drawn and calculated in EES

The results of the last option calculated in this scenario are listed in Table 11. There is not much difference in terms of cost when compared to having a central separator station in cluster F for all wells in clusters B and C, and an individual separator station in cluster A. The total cost of the selected pipeline is USD **24,800,000**.

TABLE 11: Scenario 2, single-phase pipeline scenario – individual separator station for each cluster

Line ID	Length (m)	Pipe diameter (mm)	Flow type	Fluid velocity (m/s)	Pressure drop (bar)	Cost (USD)	Cost (USD/kg of fluid)
A – A (Sep)	637	4×1000	Two phase	39.31	0.02	1,056,436	800
B – B (Sep)	448	2×1000	Two phase	38.14	-0.02	374,742	770
C – C (Sep)	1357	4×1000	Two phase	39.70	0.10	2,225,772	2195
A (Sep) – F	4789	6×900	Steam	27.82	0.78	9,418,002	28518
B (Sep) – F	2564	2×1000	Steam	34.51	0.58	2,093,018	11914
C (Sep) – F	3328	7×900	Steam	36.39	0.51	7,646,674	16045
A (Sep) – D	3313	1×850	Brine	1.72	-15.42	826,724	1101
B (Sep) – E	5045	1×500	Brine	1.63	-30.27	772,243	2472
C (Sep) – D	1805	1×700	Brine	1.91	-17.32	431,238	851

For Line A (Sep) - F, the pressure drop is too large and even increasing the number of pipes just increases the total cost with no significant reduction in pressure drop. Hence it can be deduced that it may not be economical to have a steam pipeline from cluster A to cluster F. Calculation results are presented in Figure 17.

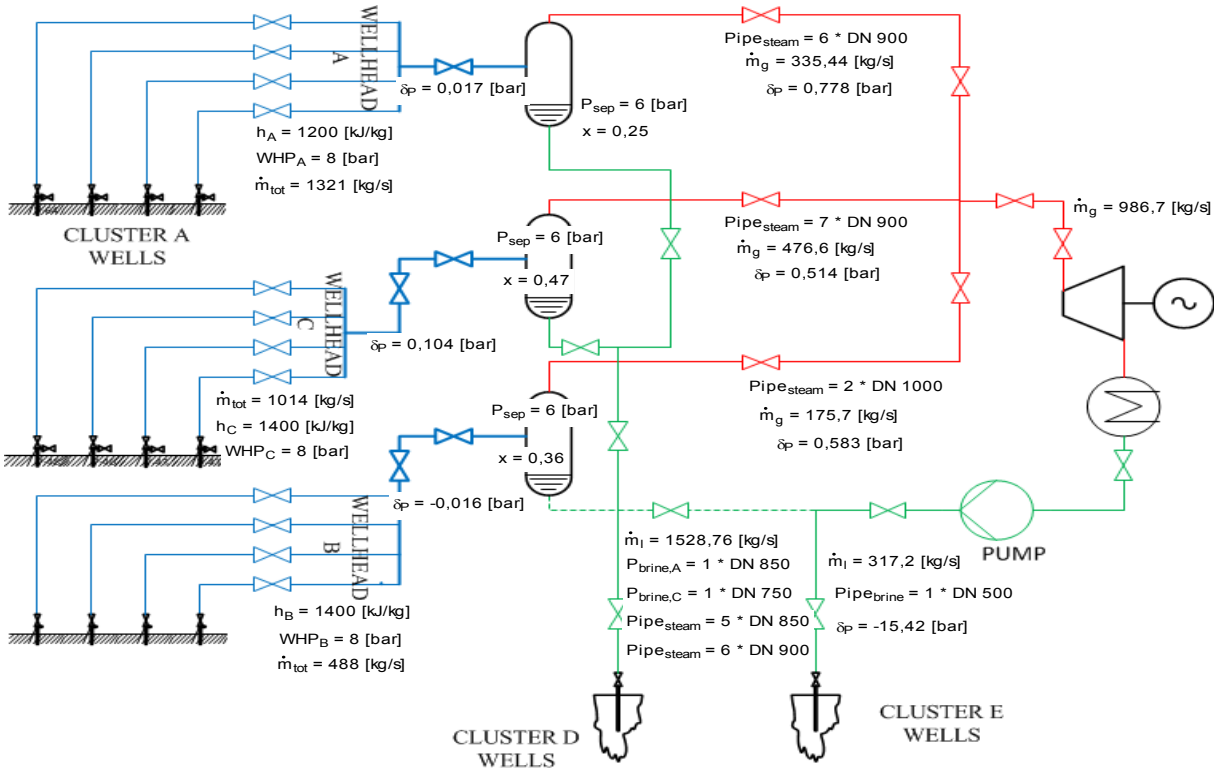

FIGURE 17: Scenario 2 results, individual separator station at each cluster A, B, and C, drawn and calculated in EES

3.3.3 Scenario 3 results

In this scenario, the power plants are located in clusters A and F with individual separator stations in clusters A, B and C. All steam from cluster B goes to cluster F while steam in cluster C is divided between clusters A and F. Brine from clusters A and C is re-injected to cluster D while brine from cluster B is re-injected in cluster E. The results are shown in Table 12. It offers a cheaper alternative when compared to all options calculated for Scenario 2.

TABLE 12: Scenario 3 results

Line ID	Length (m)	Pipe diameter (mm)	Flow type	Fluid velocity (m/s)	Pressure drop (bar)	Cost (USD)	Cost (USD/kg of fluid)
A – A (Sep)	637	4×1000	Two phase	39.31	0.02	1,056,436	800
B – B (Sep)	448	2×1000	Two phase	38.14	-0.02	374,742	770
C – C (Sep)	1357	4×1000	Two phase	39.70	0.10	1,639,548	1617
A (Sep) – D	3313	1×850	Brine	1.72	-15.42	826,724	1101
C (Sep) – D	1805	1×700	Brine	1.91	-17.32	431,238	851
B (Sep) – E	5045	1×500	Brine	1.63	-30.27	772,243	2472
B (Sep) – F	2564	2×1000	Steam	34.51	0.58	1,539,194	8551
C (Sep) – F 0.6 of m_{tot}	3328	4×1000	Steam	30.83	0.50	5,426,836	18,978
C (Sep) – A	1635	3×900	Steam	35.31	0.46	1,617,918	8487

The total cost of the selected pipeline costs is USD **13,700,000.** Figure 18 shows a cost comparison of different pipelines as a function of the total cost. A steam pipeline from cluster C takes the largest share of the cost, due to longer pipe routes.

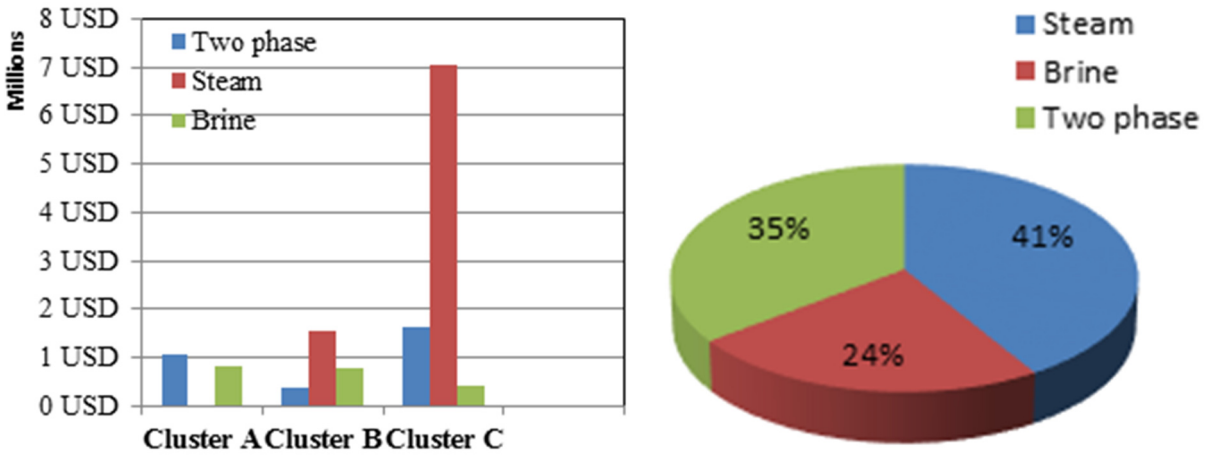

FIGURE 18: Charts showing pipeline costs based on clusters (on the left) and pipe fluid type (on the right)

Figure 19 shows the calculation results from EES.

3.4 Final results for Menengai pipelines

According to the calculations of the different scenarios, the best pipeline configuration appears to be a hybrid pipeline system with power plants in cluster A and a central separator station in cluster A for cluster A and C wells, and an individual separator station in cluster B. All brine from clusters A and C

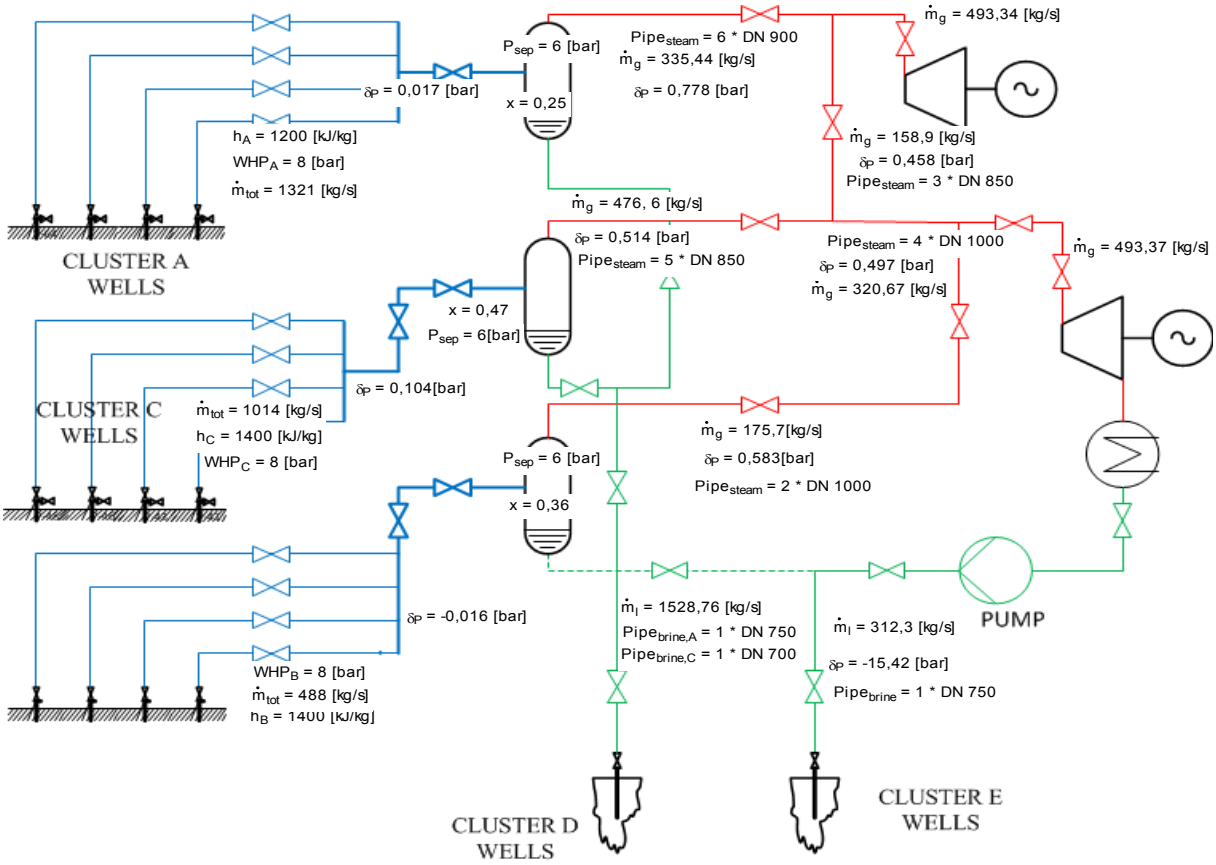

FIGURE 19: Individual separator station in each cluster and power plants in clusters F and A, drawn and calculated in EES

is re-injected in cluster D while brine from cluster B is re-injected in cluster E. The total cost of the pipeline of this chosen option is USD **9,300,000.** Figure 20 shows cost as a percentage for having power plants in cluster A while having an individual separator station in each cluster and also the cost for when wells in clusters A and C have a central separator station at A while cluster B wells have a separator station in cluster B. It can be seen that having an individual separator station in each cluster increases the pipeline cost by about 20%.

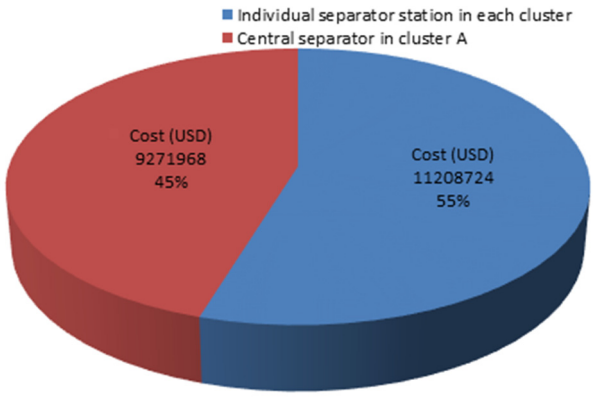

FIGURE 20: Chart showing cost comparison for the two options calculated in Scenario 3

Scenario 3 can also give better alternatives when the power plants are not located centrally due to other factors that that may arise in future. However, the cost would, increase by almost 50%.

3.5 Expansion loops results

Both u shape and change of direction expansion loops were calculated and may be used although their use may be limited as the pipeline routes used in this study are just preliminary and the routes may change as more wells are being drilled and other infrastructure made. U shape expansion loops were calculated using the Kellogg chart attached in Appendix I. The results are shown in Tables 13 and 14.

TABLE 13: Calculation results for U-shape expansion loops

Cluster	Pipe ID	Scheme	Fluid	NPD (mm)	T (mm)	L_s (m)	U-shape expansion loop (m)					Cost (USD)
							L_{anc}	L	L_c	K_1.L	K_2.L	
Brine pipelines												
A		1 pipe	Brine	850	8.8	19	200	35	9	18	5	826,724
		2 pipes		600	6.3	25	200	25	6	13	7	1,113,062
B	B-E	1 pipe	Brine	500	6.3	27	200	27	7	14	6	772,243
C	C-D	1 pipe	Brine	700	8.8	20	200	20	5	10	9	431,238
Steam pipelines												
A	A-F	4 pipes	Steam	1000	8.8	28	200	82	21	41	5	9,418,002
B	B-A	2 pipes	Steam	1000	8.8	28	200	82	21	41	5	2,078,402
	B-F	2 pipes	steam	1000	8.8	28	200	82	21	41	5	2,093,018
C	$C-A_1$	6 pipes	steam	1000	8.8	28	200	82	21	41	5	3,253,392
		3 pipes	steam	900	8.8	29	200	71	18	36	5	1,617,918
	C-F	6 pipes	steam	1000	8.8	28	200	82	21	41	5	7,646,674
Two-phase pipelines												
A	A-Sep	4 pipes	Two phase	1000	8.8	16	200	75	19	38	6	1,056,436
	A-F	4 pipes		1000	8.8	16	200	75	19	38	6	11,046,152
B	B-Sep	2 pipes	Two phase	1000	8.8	16	200	75	19	38	6	374,742
	B-F	2 pipes		1000	8.8	16	200	53	13	27	6	2,093,018
C	C-Sep	4 pipes	Two phase	1000	8.8	16	200	75	19	38	6	1,639,548
	C-A	4 pipes		1000	8.8	16	200	75	19	38	6	2,677,268
	C-F	4 pipes		1000	8.8	16	200	75	19	38	6	8,724,080

TABLE 14: Calculation results for change of direction expansion loop

Cluster	Pipe ID	Scheme	Fluid	NPD (mm)	T (mm)	L_s (m)	Change of direction expansion loop (m)					Cost (USD)
							L_{anc}	U	L_{arm}	L_{sv}	L_{sh}	
Brine pipelines												
A	A-D	2 pipes	Brine	900	8.8	17	101	69	49	17	48	2,144,590
		1 pipe		850	8.8	19	64	50	35	19	35	826,724
B	B-E	1 pipe	Brine	500	6.3	27	64	38	27	17	27	772,243
C	C-D	1 pipe	Brine	700	8.8	20	23	29	20	20	20	431,238
Steam pipelines												
A	A-F	4 pipes	Steam	1000	8.8	28	263	117	82	28	82	9,418,002
B	B-A	2 pipes	Steam	1000	8.8	28	263	117	82	28	82	2,078,402
	B-F	2 pipes	Steam	1000	8.8	28	263	117	82	28	82	2,093,018
C	C-A_1	6 pipes	Steam	1000	8.8	28	263	117	82	28	82	3,253,392
		3 pipes	Steam	900	8.8	29	217	100	71	29	71	1,617,918
	C-F	6 pipes	Steam	1000	8.8	28	263	117	82	28	82	7,646,674
Two-phase pipelines												
A	A-Sep	4 pipes	Two phase	1000	8.8	25	141	106	75	25	75	1,056,436
	A-F	4 pipes		1000	8.8	25	141	106	75	25	75	11,046,152
B	B-Sep	2 pipes	Two phase	1000	8.8	25	141	106	75	25	75	374,742
	B-F	2 pipes		1000	8.8	25	110	75	53	16	53	2,093,018
C	C-Sep	4 pipes	Two phase	1000	8.8	25	141	106	75	25	75	1,639,548
	C-A	4 pipes		1000	8.8	25	141	106	75	25	75	2,677,268
	C-F	4 pipes		1000	8.8	25	141	106	75	25	75	8,724,080

4. PRELIMINARY SIZING OF SEPARATORS

4.1 Sizing and cost of separators

The separation pressure should be selected based on silica concentration temperatures to avoid silica scaling. Silica scaling in well MW-01 can only occur when the fluid is cooled to below 80°C (Kipng'ok, 2011), hence for cluster A wells, a separator pressure of as low as 1 bar can be used since there are no dangers of silica scaling. Low separation pressures are desirable to accommodate any future decline in pressures in production wells and also to increase the steam quality. On the other hand, high separation pressures result in low steam output but high-pressure steam. Separators will be designed based on the scenarios discussed in the pipeline design section.

Central separator stations at power plant sites
The results for central separation station for all wells are presented in Table 15. Based on these results, due to low outlet steam velocity, it is better to have small separator units as the outlet steam quality increases when the total flow rate is reduced (small separator).

TABLE 15: Results for centralized separator station

Number of separators	**1**	**2**	**3**	**4**	**10**	**15**	**20**
D (m)	10.39	7.35	6.001	5.197	3.287	2.684	2.324
D_e (m)	3.15	2.275	1.818	1.575	0.996	0.8132	0.7043
D_b (m)	3.15	2.275	1.818	1.575	0.996	0.8132	0.7043
α (m)	-0.472	-0.334	-0.273	-0.236	-0.149	-0.122	-0.106
z (m)	17.32	12.25	10	8.661	5.478	4.473	3.874
β (m)	11.02	7.795	6.365	5.512	3.486	2.846	2.465
Centrifugal efficiency, η_m (%)	96.01	97.13	97.70	98.05	98.93	99.22	99.39
Entrainment efficiency, η_A (%)	99.99	99.99	99.99	99.99	99.99	99.99	99.99
Efficiency, η (%)	96.01	97.13	97.70	98.05	98.93	99.21	99.39
Outlet steam quality, x_o (%)	93.09	94.95	95.90	96.5	98.06	98.57	98.87
Pressure drop, ΔP (kPa)	25.018	25.018	25.018	25.018	25.018	25.018	25.018
Thickness, t (mm)	32.48	22.97	18.75	16.24	10.27	7.79	7.264

Individual separator stations at each cluster
Table 16 shows the results for a separator station at each cluster. It can be seen that having large central separators results in low separation efficiency and poor outlet steam quality. Thus, having smaller

TABLE 16: Results for individual separator stations per cluster

	Cluster A			**Cluster B**			**Cluster C**		
Number of separators	4	5	10	4	5	10	4	5	10
D (m)	3.029	2.709	1.916	2.161	1.933	1.367	3.115	2.786	1.97
D_e (m)	0.9178	0.8209	0.5805	0.655	0.5856	0.414	0.944	0.8442	0.5969
D_b (m)	0.9178	0.8209	0.5805	0.655	0.5856	0.414	0.944	0.8442	0.5969
α (m)	-0.138	-0.123	-0.087	-0.10	-0.088	-0.06	-0.14	-0.127	-0.089
z (m)	5.048	4.515	3.193	3.601	3.221	2.278	5.191	4.643	3.283
β (m)	3.212	4.136	2.032	2.29	2.05	1.231	3.303	2.955	2.089
Centrifugal efficiency, η_m (%)	99.37	99.48	99.73	99.46	99.56	99.79	99.02	99.12	99.54
Entrainment efficiency, η_A (%)	99.99	99.99	99.99	99.99	99.99	99.99	99.99	99.99	99.99
Efficiency, η (%)	99.37	99.48	99.73	99.46	99.56	99.78	99.02	99.47	99.54
Outlet steam quality, x_o (%)	98.18	98.5	99.21	99.00	99.18	99.59	98.21	98.48	99.15
Pressure drop, ΔP (kPa)	28.95	28.95	25.02	25.02	25.02	25.02	28.95	28.95	25.02
Thickness, t (mm)	9.47	8.47	5.99	6.75	6.04	4.232	9.73	8.71	6.16

separation units near the wells may result in higher steam outlet quality, but the cost of the separator units would increase.

4.2 Total cost of separators

For a central separation station, the mixture inlet pipe diameter (D_t) is restricted to 500-1000 mm and, based on this, the number of separators needed is calculated from which the total cost can be calculated. Here, only three cases were considered, based on the number of separators. The results are shown in Tables 17 and 18.

TABLE 17: Cost for separators in USD (individual separator stations in each cluster)

No. of separators	**4**			**5**			**10**		
Cluster	A	B	C	A	B	C	A	B	C
Steel material cost	120,832	43,868	131,396	108,075	39,240	117,525	76,420	27,750	83,100
Insulation material and cover cost	32,208	10,967	32,849	27,019	9,810	29,381	19,105	6,938	20,775
Total cost	**153,040**	**54,835**	**164,245**	**135,094**	**49,050**	**146,906**	**95,525**	**34,688**	**103,875**

In the case of individual separation station for each cluster, the total cost was calculated and shown in the table for each cluster.

TABLE 18: Cost for separators in USD (centralized separation station in clusters F and A)

No of separators	**10**		**15**		**20**	
Separator location	Cluster A	Cluster F	Cluster A	Cluster F	Cluster A	Cluster F
Steel material cost	290,400	386,030	237,870	315,195	205,340	272,960
Insulation material and cover cost	72,600	96,508	59,468	78,799	51,335	68,240
Total cost	**363,000**	**482,538**	**297,338**	**393,994**	**256,675**	**341,200**

5. PRELIMINARY SIZING OF REINJECTION PUMPS

A sump pit should be constructed near the re-injection pumps so that waste water from the separator stations can flow to the sump pits by gravity head alone. An overflow pond should also be provided alongside the reinjection sump to allow for periods of pump failure. The total brine flow from all the separator stations is 1841 kg/s, however pumping will only be required when separator stations are located in cluster F and the brine has to be pumped to clusters D and E for reinjection; in all other cases, the brine can flow by gravity.

5.1 Sizing and cost of pumps

With the reinjection wells located in clusters D and E, the pumping requirement for the reinjection pumps can be calculated using the following equation (Jónsson, 2012):

$$W_p = \frac{g\, m_f\, \Delta P\, 100}{\eta} \tag{68}$$

where W_p = Pump power (W);
m_f = Water flow rate (kg/s);
ΔP = Total pressure head (m);

η = Pump efficiency;
g = gravity constant (m/s^2).

Assuming a pump efficiency of 85% and a water flow rate of 883 kg/s, the pumping requirement is calculated to be 1019 kW. Having four smaller units, 510 kW each, is operationally safe as two pumps would be running with the other two pumps on standby, and economical as pumps require special maintenance.

6. CONCLUSIONS AND DISCUSSION

The results show that the optimal design for the steam gathering system is having the power plants located in cluster A with a central separator station for cluster A and C wells, and an individual separator station for cluster B wells. This is followed closely by the scenario with the power plants in cluster A and individual separator stations in each cluster. Another possible solution would be to have power plants in clusters A and F and individual separator stations for clusters A, B and C.

In all the above options, the brine in clusters A and C is reinjected in cluster D, while brine from cluster B is reinjected in cluster E. There would be no pumping requirement for the brine since it would flow by gravity.

On the other side having an economical centralized separator station in Menengai is not a straight forward solution, as there are restrictions due to topography.

Calculations done in this report were based on limited data and several assumptions were made in order to get the preliminary results. These preliminary results can be used as a basis for a more detailed design for a steam gathering system once more accurate data become available.

ACKNOWLEDGEMENTS

I would like to thank UNU-GTP for the opportunity, in particular Dr. Ingvar Birgir Fridleifsson, Director, and Deputy Director Lúdvík S. Georgsson for my nomination to attend the 2012 UNU Geothermal Training Programme. I recognize the guidance and assistance offered to me by my supervisor, Professor Magnús Thór Jónsson and to Associate Professor Halldór Pálsson, both from the University of Iceland. I also want to thank Ms. Málfrídur Ómarsdóttir, Mr. Ingimar G. Haraldsson, Mr. Markús A.G. Wilde and Ms. Thórhildur Ísberg for their support throughout the entire period. My special thanks go to my employer, Geothermal Development Company Ltd. (GDC) and in particular to Mr. Cornel Ofwona, manager of Geothermal Resource Management for giving me permission to attend this training programme. I am grateful to the UNU-GTP Fellows for a fruitful time together and the friendships made.

My deepest thanks go to my wife Victoria for her sacrifice and support and my two lovely daughters, Daisy and Elleen, for enduring my long absence from home. Finally, to God: all the praise and glory for the successful completion of the training programme.

REFERENCES

ASME, 1974: *ASME boiler and pressure vessel code.* American Society of Mechanical Engineers.

Chexal, B., Horowitz, J., McCarthy, G., Merilo, M., Sursock, J.P., Harrison, J., Peterson, C., Shatford, J., Hughes, D., Ghiaasiaan, M., Dhir, V., Kastner, W., and Köhler, W., 1999: *Two-phase pressure drop technology for design and analysis*. EPRI, Inc., Palo Alto, CA, Final Report, 304 pp.

Chisholm, D., 1983: *Two-phase flow in pipelines and heat exchangers*. The Institution of Chemical Engineers, NY, 304 pp.

DiPippo, R., 2007: *Geothermal power plants. Principles, applications, case studies and environmental impact* (2nd ed.). Butterworth Heineman, Elsevier, 493 pp.

F-Chart Software, 2012: *EES, Engineering Equation Solver*. F-Chart Software, website, *www.fchart.com/ees/ees.shtml.*

Jónsson, M.Th., 2012: *Mechanical design of geothermal power plants*. UNU-GTP, Iceland, unpublished lecture notes.

Kellogg, M.W., 1956: *Design of piping systems* (rev. 2nd edition). John Wiley & Sons, Inc., NY, USA, 385 pp.

Kipng'ok, J.K., 2011: Fluid chemistry, feed zones and boiling in the first geothermal exploration well at Menegai, Kenya. Report 15 in: *Geothermal training in Iceland 2011*. UNU-GTP, Iceland, 281-302.

Lazalde-Crabtree, H., 1984: Design approach of steam-water separators and steam dryers for geothermal applications. *Geothermal Resources Council, Bulletin, Sept. 1984,* 11-20.

Muchemi, G.M., 1998: Geothermal exploration in the Kenya rift. In: Georgsson, L.S., (editor), *Geothermal training in Iceland, 20th Anniversary Workshop 1998.* UNU-GTP, Iceland, 121-130.

Ngugi, P.K., 2012: Kenya's plans for geothermal development – a giant step forward for geothermal. *Presented at the "Short Course on Geothermal Development and Geothermal Wells", organized by UNU-GTP and LaGeo, Santa Tecla, El Salvador*, 8 pp.

Ofwona, C.O., 2004: *Heat loss assessment of Menengai – Olbanita geothermal prospect*. KenGen, Kenya, internal report, 19 pp.

Simiyu, S.M., 2009: Application of micro-seismic methods to geothermal exploration: Examples from the Kenya rift. *Paper presented at "Short Course IV on Exploration for Geothermal Resources", organized by UNU-GTP, KenGen and GDC, Lake Naivasha, Kenya,* 27 pp.

Thome, J. (ed.), 2006: *Engineering data, book III.* Wolverin Tube Inc., Lausanne, Switzerland.

Walas, S.M., 1990*: Chemical process equipment, selection and design*. Butterworth-Heinemann, Washington, USA, 755 pp.

Zhao H.D., Lee, K.C., and Freeston, D.H. 2000: Geothermal two-phase flow in horizontal pipes, New Zealand. *Proceedings of the World Geothermal Congress 2000, Kyushu-Tohoku, Japan*, 3349-3352.

APPENDIX I: The M.W. Kellogg U-shape expansion loop chart (Kellogg, 1956)

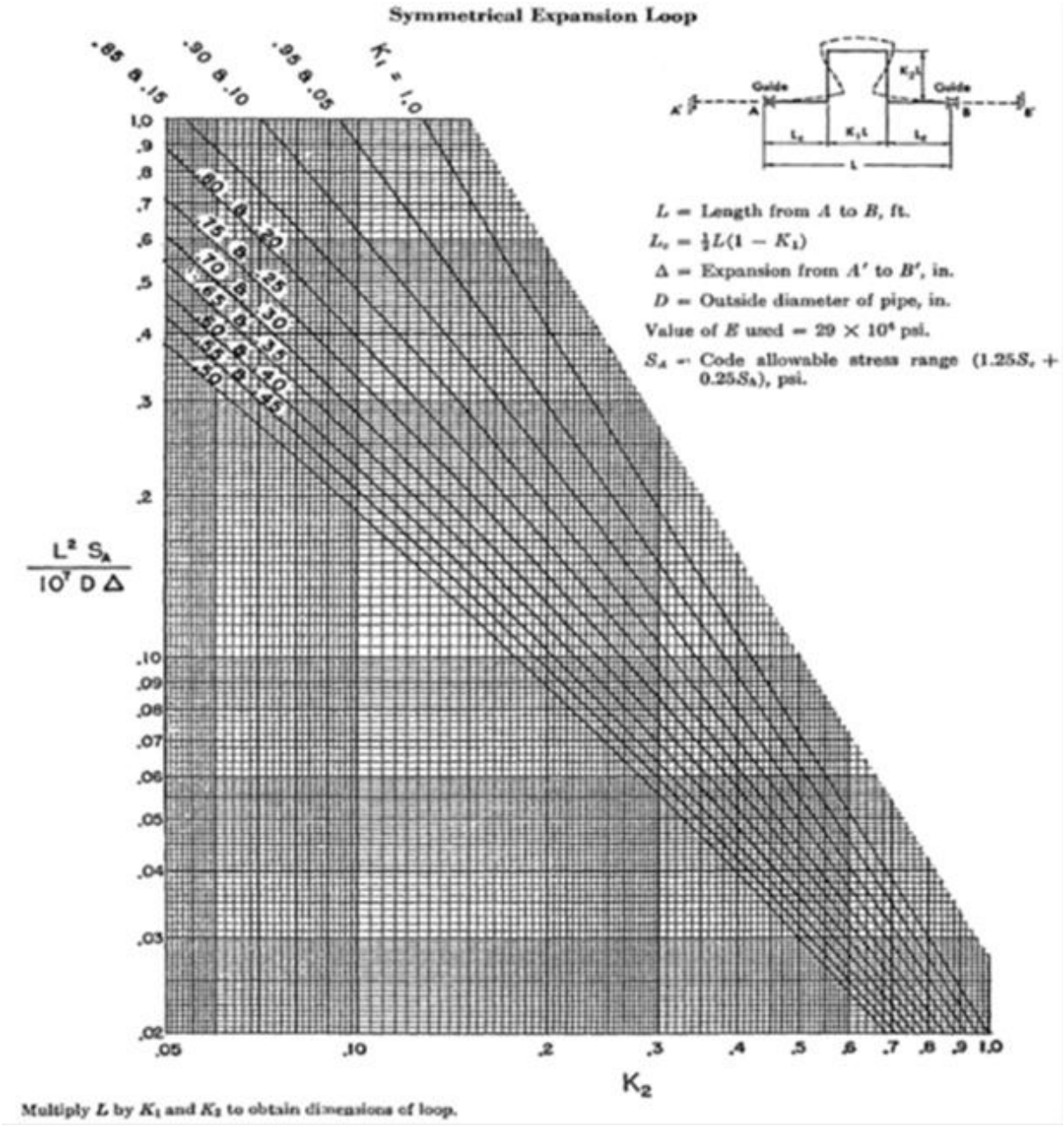

FIGURE 1: Kellogg U-shape expansion loop chart

APPENDIX II: Well test productivity indices, temperature and pressure plots

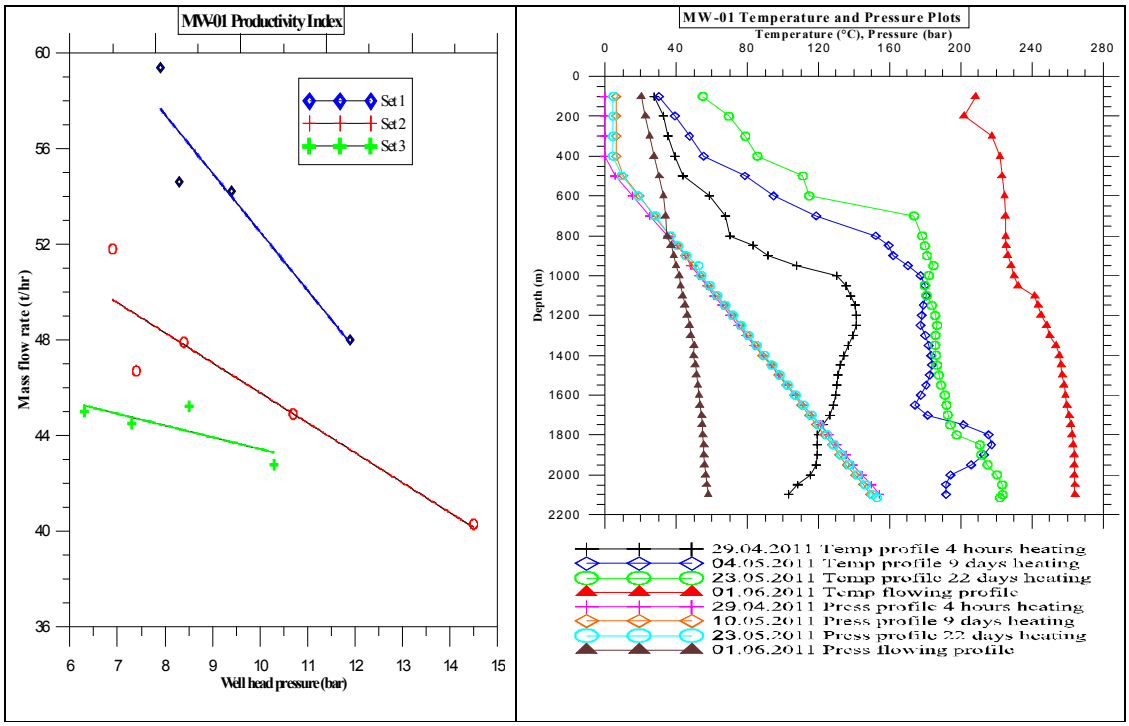

FIGURE 1: MW-01 Productivity index plot on the left and measured down hole temperature and pressure profiles on the right

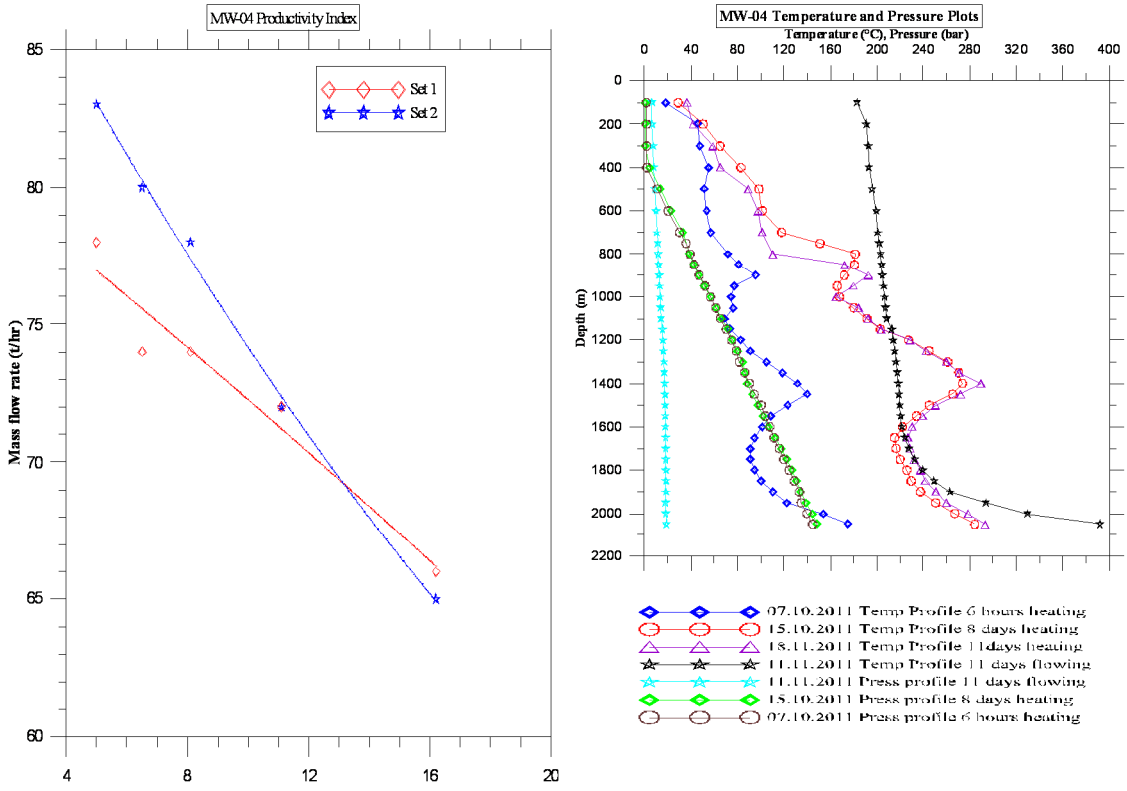

FIGURE 2: MW-04 Productivity index plot on the left and measured down hole temperature and pressure profiles on the right

APPENDIX III: An example of the EES calculations

```
"#########################################################################
#########################################################################
######## DESIGN OF THE MENENGAI PHASE I STEAM GATHERING SYSTEM##########
##################CLUSTER A CALCULATIONS ################################
################    Two phase flow pipelines calculations#################################
Stephen Onyango, UNU GTP 2012#####Two phase Pressure drop and Mechanical stress analysis"#

Procedure  friction( R_e;f_1;f_2:f)

        if R_e <= 2000 then

        f=f_1
 else
        f = f_2

 endif
 end

"############################  Two phase pipeline   ##############################"

"##############################GIVEN DATA#####################################"

P_sep = 6[bar]
h_1 = 1200[kJ/kg]
g=9,81[m/s^2]
m_dot_tot = 330,25[kg/s]
epsilon = 0,046*10^(-3)
P_1 = P_sep
D_in = 0,9984[m]
D_o = D_in + 2*t_pipe
t_pipe = lookup('lookup 1';17;'t_pipe')
L_p = 650[m]
H_e = 2065[m]
H_s=2055[m]
T_Hot =T_sat(Steam_IAPWS;P=P_1)                                  {operating temperature }
T_cold = 18[°C]
rho_l =Density(Steam_IAPWS;P=P_1;x=0)
rho_g=Density(Steam_IAPWS;P=P_1;x=1)
mu_l = Viscosity(Steam_IAPWS;P=P_1; x=0)
mu_g = Viscosity(Steam_IAPWS;P=P_1; x=1)
x =Quality(Steam_IAPWS;P=P_1;h=h_1)                                {steam quality}

m_dot_l = (1-x)*m_dot_tot
m_dot_g= x*m_dot_tot

V_g=(m_dot_g/rho_g)/A_pipe
A_pipe = (pi*D_in^2)/4
R_e= rho_l*V_bar * D_in/mu_l
 f_1 = 64/R_e
 f_2 =  0,25/(log10(epsilon/3,7*D_in+ 5,74/R_e^0,9))^2
call friction(R_e;f_1;f_2:f)
```

```
(1-alpha)/alpha^(7/8) = ((1/x-1)*(rho_g/rho_l)*(mu_l/mu_g))^(7/8)          {void fraction}

V_bar_l= (1,1*(1-x)*m_dot_tot*(1-x))/(rho_l*(1-alpha)*A_pipe)          {liquid phase velocity}
V_bar_l/V_bar = (1-sqrt(alpha)^(8/7))*(1+(8/7)*sqrt(alpha))/(1-alpha)          " average velocity "

rho_tp = (rho_g*alpha) +( rho_l*(1-alpha))                          {two phase density}

mu_tp= mu_g*x + mu_l*(1-x)                                  {two phase dynamic viscosity}

Re_tp = (rho_l* V_bar*D_in)/mu_l                            {reynold number for two phase}

H_f =( f*V_bar_l^2*L_e)/(2*g*D_in)                          "Head loss due to friction"

"##########################Equivalent length calculations##############################"

L_e=L_p+n_b*h_b*D_in+n_c*h_c*D_in+n_u*h_u*D_in+n_v*h_v*D_in {Second equivalent length}

h_b = 20*D_in
h_c =  20*D_in
h_u = 20*D_in
h_v = 10*D_in

n_b = (L_p/100) + 2
n_c = 2
n_u =  0
n_v= 2
n_d=0

"#######################pressure drop calculations#################################"

P_delta_l =(f*rho_l*V_bar^2*L_e)/(2*D_in*(1-AC))    "pressure drop due to friction on pipe length"
AC = (m_dot_g)/(rho_g*P_2*A_pipe^2*alpha)                    { acceleration correction factor}

P_2 = P_sep*100000

phi_BLOb^2= 1+ ((rho_l/rho_g) -1)*(B*x*(1-x) + x^2)    { the first two phase multipliers for bends}
B = 1 + (2,2/(K_BLOb*(2 + r/D_in)))
r = 5*D_in
K_BLOb = 1,6*f*h_b

phi_BLOc^2=1+((rho_l/rho_g)-1)*(B_c*x*(1-x)+x^2)  {the first two phase multipliers for
connections}
B_c = 1

phi_BLOu^2= 1+ ((rho_l/rho_g) -1)*(B_u*x*(1-x) + x^2) { the first two phase multipliers for
expansion units}
B_u = 1

phi_BLOv^2=1+((rho_l/rho_g) -1)*(B_v*x*(1-x) + x^2)   { the first two phase multipliers for valves}
B_v = 1
"############## pressure drop for all installations#################"

p_delta_i= (f*rho_tp*V_bar^2)*(phi_BLOb^2*n_b + phi_BLOc^2*n_c + phi_BLOu^2*n_u +
phi_BLOv^2*n_v)/2
```

"pressure drop due to installations"

p_delta_Z = rho_tp*g*Z_delta "presure drop to elavation change"
Z_delta = H_e-H_s {elavation difference}

p_delta_T =p_delta_Z+ p_delta_L + p_delta_i "Total pressure drop"

"###############Cost calculations####################"

C_c = L_p *k_p + n_b*k_b + n_c*k_c + n_u*k_u + n_v*k_v + n_d*k_d {Capital cost }

k_p = lookup('lookup 1';17;'k_p')
k_b = lookup('lookup 1';17;'k_b')
k_c = lookup('lookup 1';17;'k_c')
k_v = lookup('lookup 1';17;'k_v')
k_u = 0
k_d=0

"#################Nominal pipe thickness calculations####################"

t_m = (P*D_o)/(2*(S*E + P*y)) +A
P = P_sep*1,5
E = 0,85
A= 3/1000
S = 115*10^6
y = 0,4

"########################Sustained loads#####################################"

q_sv = q_p + q_e {vertical sustained loads}
q_p = pi*g*rho_s*((D_o^2) - (D_in^2))/4 {pipe weight}
q_e = pi*g*rho_e*((D_e^2) - (D_o^2))/4 {insulation weight}
rho_s = 7850[kg/m^3] {density of steel}
rho_e = 220[kg/m^3] {density of insulation material}
D_e = D_o + 2*t_e
t_e = (100/1000) {insulation thickness}

"####################Occasional loads###"

q_dv = q_v + q_s + q_jv {vertical occasional loads}
q_v = pi*g*rho_tp*(D_in^2/4) {rho_tp = two phase density}
q_s = 0,2*S_f*D_e
q_jv = 0,5*e_s*q_o
q_o = q_v + q_p +q_e
S_f = 0 {Snow factor=0, no snow}
e_s = 0,16 {seismic factor, from KPLC design reports}

q_dh = q_jh {horizontal occasional loads}
q_jh = e_s*q_o

"######################## Length between supports#####################################"

L_s^2 =(((k*S_h) - (P*D_o)/(4*t_m)) * (pi/4*(D_o^2 - D_in^2)))/ (D_o*0,75*i*((q_sv) + (sqrt(q_dv^2 + q_dh^2))))

```
0,75*i= 1
k= 1,15
 S_h = 115*10^6                    {Stress at 370°C}{ Allowable stress under hot conditions}

 (0,75*i)*((q_sv*L_sv^2) + sqrt((q_dv*L_sv^2)^2 + (q_dh*L_sh^2)^2))/(8*Z) =   (k*S_h) -
P*D_o/(4*t_m)

Z= (pi/32)*((D_o^4 - D_in^4)/D_o)
L_sv= L_s

"#######################Thermal expansion in pipelines#############################"

delta_L = alpha_1 * L_p* delta_T
alpha_1 = alpha_ ('Carbon_steel'; Temperature)
Temperature= T_Hot
epsilon_x = alpha_1/delta_T
delta_T= T_hot - T_cold
Sigma_x = E_y * epsilon_x
Force = A_1 * Sigma_x
E_y = 200*10^9
A_1 = pi*D_in*L_p

"###################Zig zag expansion loop#########################################"

Y_resultant/1000= alpha_1*delta_T*L_ANC
L_Developed = L_1 + L_2
U= sqrt(L_1^2+ L_2^2)
L_ANC = sqrt(L_T1^2 + L_T2^2)
{L_arm = sqrt(D_o*alpha_1*delta_T*L_ANC/71,477)}
(D_o*1000*Y_resultant)/(L_developed - U )^2 = 208,3
L_1 = L_2
L_1 = L_arm
L_1 = L_sh
L_T2 = L_arm

"#############################U-shape expansion loo#############################"

y_axis_kellog = (L_sh*3,28)^2*S_A/(10^7*D_o*39,37*delta)

S_A = (1,25*S_c + 0,5*S_h)*0,0001450377          {allowable stress range}
S_c = 137800000                                    {Allowable stress under cold conditions}

delta = 0,03*L_U
L_U = 200*3,28                                  L_U , distance between anchors, taken as 200m}
```

APPENDIX IV: Some results from the variable topology distance transform

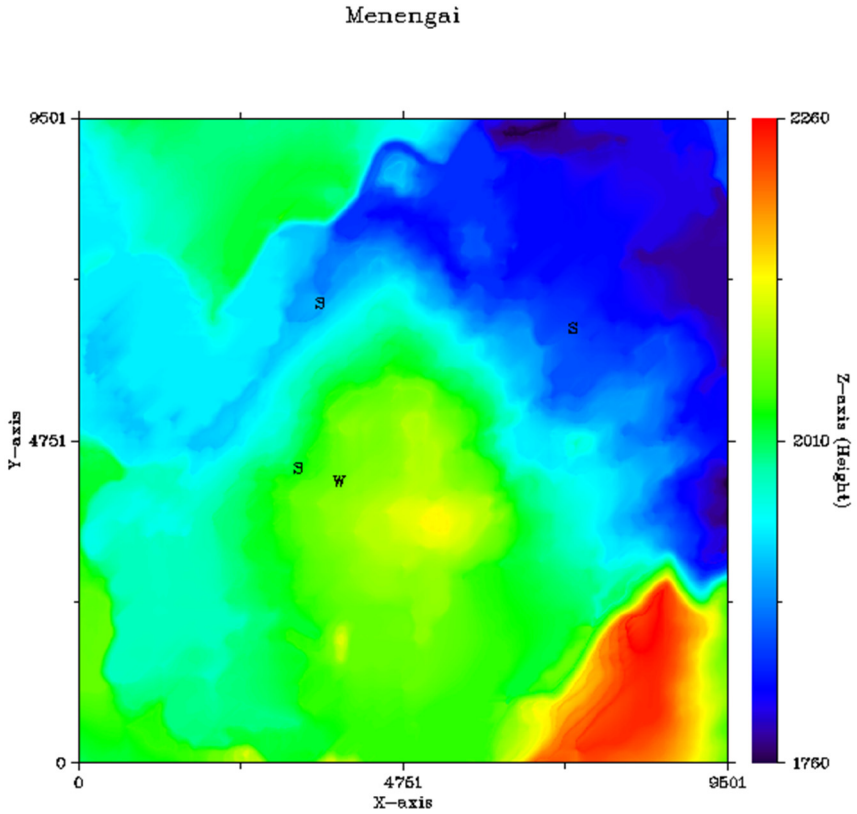

FIGURE 1: Map showing results from distance transform

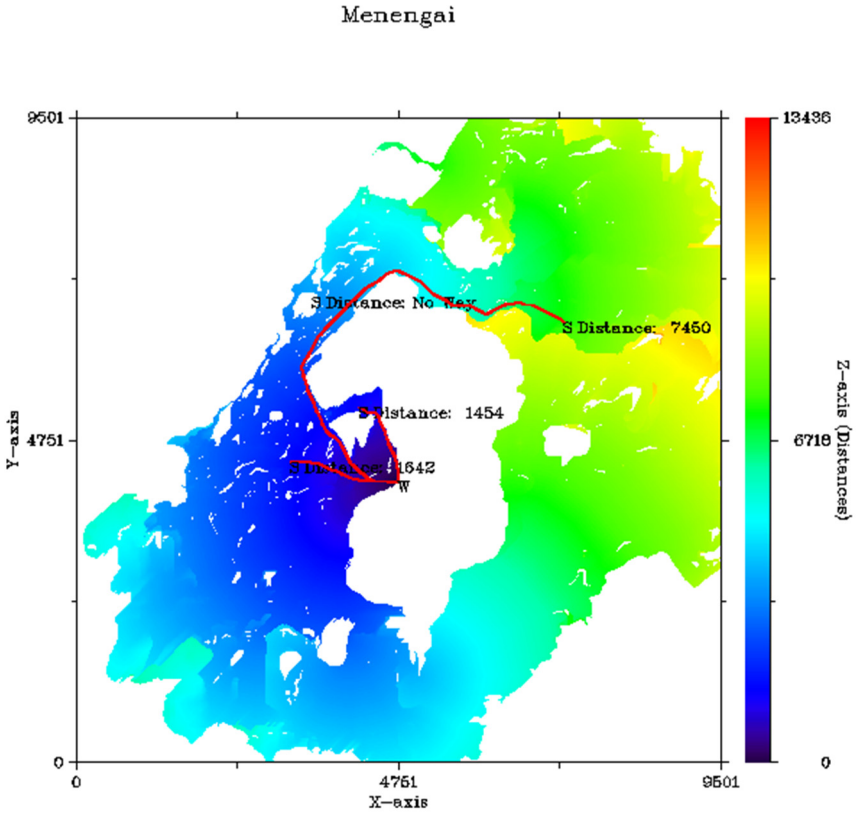

FIGURE 2: A map showing pipeline route and distance using distance transform